AD-A085 777 TRITEC INC COLUMBIA MD F/G 13/7
DEVELOPMENT OF A FLUIDIC GAS CONCENTRATION SENSOR.(U)
JUN 80 G E STEVENS, M F FUNKE DAAG39-78-C-0103
UNCLASSIFIED HDL-CR-80-103-1 NL

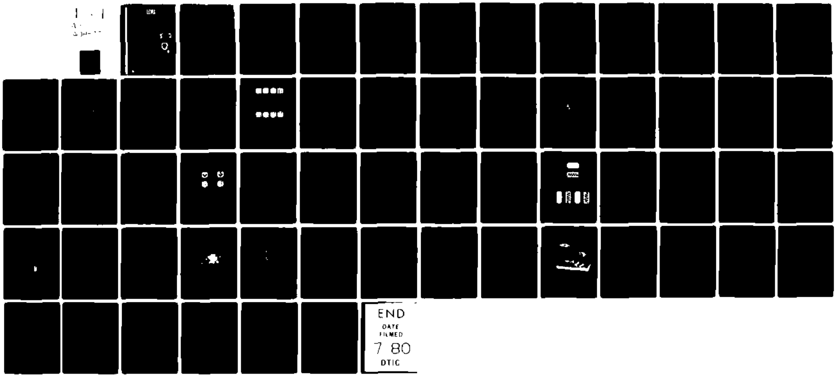

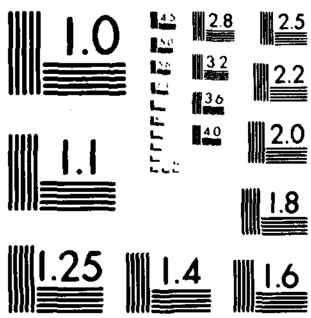

MICROCOPY RESOLUTION TEST CHART
NATIONAL BUREAU OF STANDARDS 1963 A

LEVEL II

HDL-CR-80-103

ADA085777

DEVELOPMENT OF A FLUIDIC GAS CONCENTRATION SENSOR

by George E. Stevens and Maurice F. Funke

Prepared by

TRITEC INCORPORATED
8925-11 McGaw Court
Columbia, MD 21045

Under contract

DAAG39-78-C-0103

U.S. Army Electronics Research
and Development Command
Harry Diamond Laboratories
Adelphi, MD 20783

The findings in this report are not to be construed as an official Department of the Army position unless so designated by other authorized documents.

Citation of manufacturers' or trade names does not constitute an official endorsement or approval of the use thereof.

Destroy this report when it is no longer needed. Do not return it to the originator.

UNCLASSIFIED

SECURITY CLASSIFICATION OF THIS PAGE (When Data Entered)

REPORT DOCUMENTATION PAGE

READ INSTRUCTIONS BEFORE COMPLETING FORM

1. REPORT NUMBER HDL-CR-80-103-1	2. GOVT ACCESSION NO. AD-A085 777	3. RECIPIENT'S CATALOG NUMBER Final rept.
4. TITLE (and Subtitle) DEVELOPMENT OF A FLUIDIC GAS CONCENTRATION SENSOR		5. TYPE OF REPORT & PERIOD COVERED CONTRACTOR REPORT
		6. PERFORMING ORG. REPORT NUMBER
7. AUTHOR(s) GEORGE E. STEVENS AND MAURICE F. FUNKE		8. CONTRACT OR GRANT NUMBER(s) DAAG39-78-C-0103 new
9. PERFORMING ORGANIZATION NAME AND ADDRESS TRITEC INCORPORATED 8925-11 Mc GAW COURT COLUMBIA, MARYLAND 21045		10. PROGRAM ELEMENT, PROJECT, TASK AREA & WORK UNIT NUMBERS USGS Work Order HDL Project A54734
11. CONTROLLING OFFICE NAME AND ADDRESS HARRY DIAMOND LABORATORIES 2800 POWDER MILL ROAD ADELPHI, MARYLAND 20783	16 Jun 80	12. REPORT DATE JUN 16 1980
		13. NUMBER OF PAGES
14. MONITORING AGENCY NAME & ADDRESS (if different from Controlling Office) 59		15. SECURITY CLASS. (of this report) UNCLASSIFIED
		15a. DECLASSIFICATION/DOWNGRADING SCHEDULE

16. DISTRIBUTION STATEMENT (of this Report)

APPROVED FOR PUBLIC RELEASE: DISTRIBUTION UNLIMITED

17. DISTRIBUTION STATEMENT (of the abstract entered in Block 20, if different from Report)

18. SUPPLEMENTARY NOTES

Due to transducer calibration, the non-SI unit mmHg has been substituted for the SI unit KP_a.

19. KEY WORDS (Continue on reverse side if necessary and identify by block number)

FLUIDICS	CHEMICAL PROCESSORS
FLUIDIC TECHNOLOGY	HEAT EXCHANGER
FLUIDIC SENSORS	GAS CONCENTRATION SENSORS

20. ABSTRACT (Continue on reverse side if necessary and identify by block number)

This document is the final report of a program to design, test, and evaluate the performance of fluidic gas concentration sensing systems and their component parts for monitoring C_xH_y and H_2S on offshore platforms. This program consisted of investigating three major portions of a system.

- Gas Sensors,
- Chemical Processors,
- Sensor Systems

(OVER)

DD FORM 1 JAN 73 1473 EDITION OF 1 NOV 65 IS OBSOLETE

UNCLASSIFIED 393775

SECURITY CLASSIFICATION OF THIS PAGE (When Data Entered)

Three candidate fluidic sensors were evaluated for use in the sensor system.

- Resistor Bridge Sensor
- Vortex Sensor
- Jet Edge Resonator Oscillator Sensor

The resistor bridge sensor was chosen as the most appropriate.

Several chemical processors were evaluated for each gas sensing system. Palladium coated alumina was chosen for the C_xH_y system and lead acetate was chosen for the H_2S system.

Two systems were considered, one to sense hydrocarbons (C_xH_y) and another to sense hydrogen sulfide (H_2S). The C_xH_y sensor system appeared to have the predicted sensitivity in the range from 0.01% to 2.5% methane in air. However, the signal could not be maintained for more than several minutes. The H_2S sensor system was not able to resolve H_2S concentrations in the range required due to the bridge sensor noise level.

The major find of this project is that the feasibility of the basic approach has been demonstrated and a number of problems have been identified which must be overcome before the gas sensor systems are ready for field testing.

FOREWORD

This document is the final report of a program to design, test and evaluate the performance of fluidic gas concentration sensing systems and their various components. This effort was sponsored by the U.S. Geological Survey and conducted under Contract No. DAAG39-78-C-0103 from the Harry Diamond Laboratories. We would like to thank the staff at Harry Diamond Laboratories for their assistance in many phases of this project and especially the contributions by Mr. A. Holmes of HDL and Mr. J. Gregory of USGS.

page 4 blank

CONTENTS

FIGURES

PRECEDING PAGE BLANK-NOT FILMED

FIGURES (Cont'd)

TABLES

1. INTRODUCTION

1.1 Design Objectives

The threat of gas leaks around offshore drilling and production platforms is always present. For this reason, systems for sensing combustible gas (and, if appropriate, toxic gas) are located at various points on the platforms. These systems must operate reliably under a variety of environmental conditions, while being able to discriminate between H_2S in concentrations of a few parts per million and unanticipated background gases of higher concentrations.

Fluidic gas sensors use devices that have no moving parts or sophisticated electronics, and thus offer high reliability in adverse environments. The basic fluidic gas sensing technique (Figure 1) is designed to (1) draw a sample of gas, (2) split the sample into two identical parts, (3) use a portion of the sample as the sample gas, (4) pass the other half through a chemical processor which only produces a reaction with the gas of interest to supply a reference gas, (5) minimize any temperature difference between the two gas streams, and (6) measure the resultant change of bulk gas properties with an appropriate sensor.

Three candidate fluidic sensors were investigated: the jet edge resonator oscillator, vortex sensor, and resistance bridge sensor. This program had as its goal the theoretical and experimental investigation to determine the capability of these fluidic gas-concentration sensors to detect toxic and combustible gases in an offshore environment.

The specific operational requirements of such a fluidic system are to (1) detect hydrogen sulfide (H_2S) with an accuracy of ± 5 parts per million (ppm) concentration by volume over a range of 0 to 50 ppm, and (2) detect hydrocarbons (C_xH_y) with an accuracy of $\pm\frac{1}{2}\%$ over a range of 0 to 3%.

1.2 Summary

The program consisted of a four phase effort. These phases included the design, fabrication, test, and evaluation of the following:

- chemical processors
- gas sensors
- heat exchanger
- sensor systems

The first three phases were conducted simultaneously and the results of those efforts are presented in Sections 2, 3, and 4. The fourth phase of the program, including the design, fabrication, test, and evaluation of the sensor systems, combined the results of the first three phases. The results of the fourth phase are presented in Section 5.

At the completion of the evaluation of the three fluidic gas sensors, the resistor bridge was chosen as most appropriate to fulfill the objectives of this effort. It has a gas-sensing threshold (signal level equivalent to noise) of ± 120 ppm of carbon dioxide in nitrogen. (Theory suggests that this is equivalent to ± 112 ppm of carbon dioxide in air and ± 111 ppm of H_2S in air. See Section 2.1) The signal level

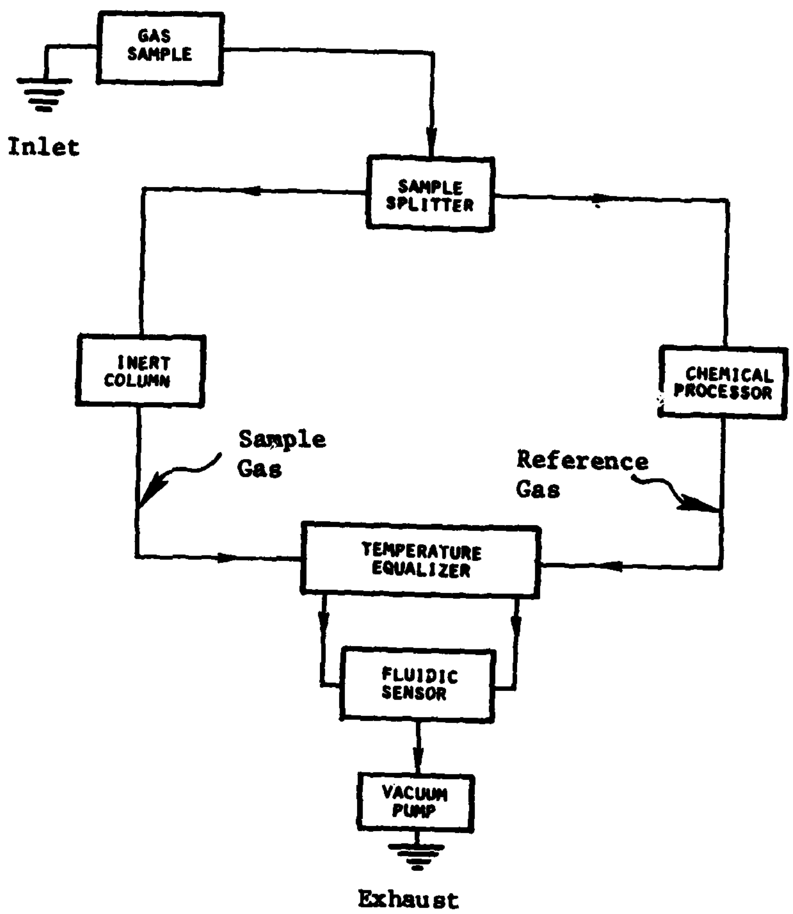

Figure 1. Diagram of fluidic gas sensing system

is more than adequate for amplification by standard fluidic amplifiers so that inexpensive electronic transducers can be used if desired.

A compact heat exchanger designed to be compatible with the pressure-flow requirements of the sensor system was evaluated and found to have the capacity of reducing temperature differences of up to 100°C in the two gas streams to a difference as low as ± 0.02°C. This capability is more than adequate for the sensor system requirements.

The action required of the chemical processor depends upon what the particular gas to be sensed is, as well as what other gases may be present in the gas sample. Four chemical processors (two for each of the two gas sensing systems evaluated in this program) were evaluated. For the H_2S sensing system, a processor was chosen that utilizes the reaction of lead acetate with H_2S from the gas stream. Testing with a gas chromatograph indicated that this processor removes 100% of the H_2S from the gas stream at operational pressure, flow and temperature conditions.

For the hydrocarbon-sensing system, the processor chosen utilizes palladium coated alumina beads (similar to those used in catalytic converters for automotive exhaust systems) to oxidize the hydrocarbons and form carbon dioxide and water vapor. Testing a methane-in-air gas mixture with a gas chromatograph indicated that this processor oxidizes nearly 100% of the hydrocarbon in the gas mixture at operational pressure, flow and temperature conditions.

Combining the components chosen in the first three phases, two complete gas sensing systems were tested. As expected, the first system was unable to sense H_2S in the 0 to 50 ppm range. This is due to a noise level in both the sensor and the amplifier that was greater in magnitude than the signal produced by 50 ppm of H_2S in air.

When the second complete system was tested, over a concentration range of 0 to 2.5% methane in air, it was capable of sensing ± 0.01% (100 ppm) methane in air. This is more than sufficient for its intended application. However, one serious drawback still exists in this system. The signal produced is transitory in nature. When a steady flow of methane and air is introduced, the signal holds steady for 1-1/2 minutes at the correct reading. It then slowly decreases back to zero over the next 8 to 10 minutes, where it remains until the methane mixture is changed or removed. When the mixture is removed, the signal then decreases in magnitude by an amount equivalent to the original signal, holds steady for about 1-1/2 minutes, and then increases slowly back to zero over the next 8 to 10 minutes.

2. FLUIDIC SENSORS

Three different types of fluidic sensors were evaluated during this program. These were the resistor bridge, the vortex sensor, and the oscillator. Based upon the theory of operation of each device, prototype models of both the bridge and oscillator were designed, tested, and evaluated. A third type of device, the vortex sensor, was tested and evaluated by NEOS, Inc. of Lincoln, Nebraska.

The results of these efforts are presented in detail in the following sections. An overall comparison of important sensor characteristics is given on Tables I and II. Each of the sensors and their operating characteristics is discussed in Sections 2.1 through 2.3.

2.1 Resistor Bridge

The resistor bridge sensor is made up of two flow paths. Each path consists of one linear (viscosity dependent) and one nonlinear (density dependent) fluid resistor placed in series, as shown in Figure 2. A sample gas mixture, containing an unknown concentration of the gas to be sensed, flows through one set of resistors, while a reference gas mixture, consisting of the sample gas as altered by the chemical processor, flows through the second set of resistors. The two flow paths are joined in a common manifold as they exit the orifice resistors. A vacuum is applied to this exhaust manifold so that the gases needed to make up the sample and reference streams can be drawn into the sensor system from ambient. The bridge differential pressure output signal is fluidically amplified with a TRITEC AM-12B five-stage proportional amplifier.

An ideal linear resistor is characterized by

$$P_L = a\mu Q, \qquad (1)$$

where

P = pressure drop across resistor (subscript L denotes a linear resistor),

$a = \dfrac{12L}{wd^3}$,

L = resistor length,

w = resistor width,

d = resistor depth,

μ = gas absolute viscosity, and

Q = volume flow through resistor.

An ideal nonlinear resistor (orifice) is characterized by

$$P_N = b\,\rho Q^2, \qquad (2)$$

where

$b = \dfrac{1}{2A^2 C_d{}^2}$,

A = orifice area,

C_d = orifice discharge coefficient,

ρ = gas density, and

subscript N denotes a nonlinear resistor.

TABLE I. MEASURED SIGNAL AND NOISE LEVEL FOR FLUIDIC SENSORS

SENSOR	TYPE OF OUTPUT SIGNAL	SIGNAL EXPECTED FROM 5 ppm H_2S in AIR ***	SIGNAL NOISE LEVEL EQUIVALENT PPM H_2S IN AIR
BRIDGE	Pressure Difference	1.60×10^{-5} mmHg	111
VORTEX	Pressure Difference	1.25×10^{-7} mmHg	32*
OSCILLATOR	Frequency Ratio Difference	6.45×10^{-7}*	170**

* This value was calculated from theory not measured
** 7.1 second signal sample time
*** Based on data taken at higher concentrations

TABLE II. CALCULATED NULL AND GAIN SENSITIVITY TO VARIATIONS IN SENSOR OPERATING CONDITIONS

SENSOR \ PARAMETER VARIED		AVERAGE TEMPERATURE (50°C CHANGE)	TEMPERATURE DIFFERENCE (10^{-3}°C DIFFERENCE)	SUPPLY PRESSURE (5% CHANGE)	CARRIER GAS PROPERTIES[a] (1% CHANGE)			
					ρ	μ	C_v	C_p
Bridge	Null change (ppm H_2S in Air)	0	3.1	3,125 ppm[b]	0	0	0	0
	Gain change (%)	6.7	0	7.0	1.3	1.5	0	0
Vortex	Null change (ppm H_2S in Air)	0	19	0[b]	0	0	0	0
	Gain change (%)	17.0	0	10[b]	5.7	0	0	0
Oscillator	Null change (ppm H_2S in Air)	0	13	13,178 ppm[b]	0	0	0	0
	Gain change (%)	10.6	0	0	-	0	-	-

a ρ = Density
μ = Viscosity
C_v = Molal specific at constant volume
C_p = Molal specific at constant pressure

b Value experimentally determined.

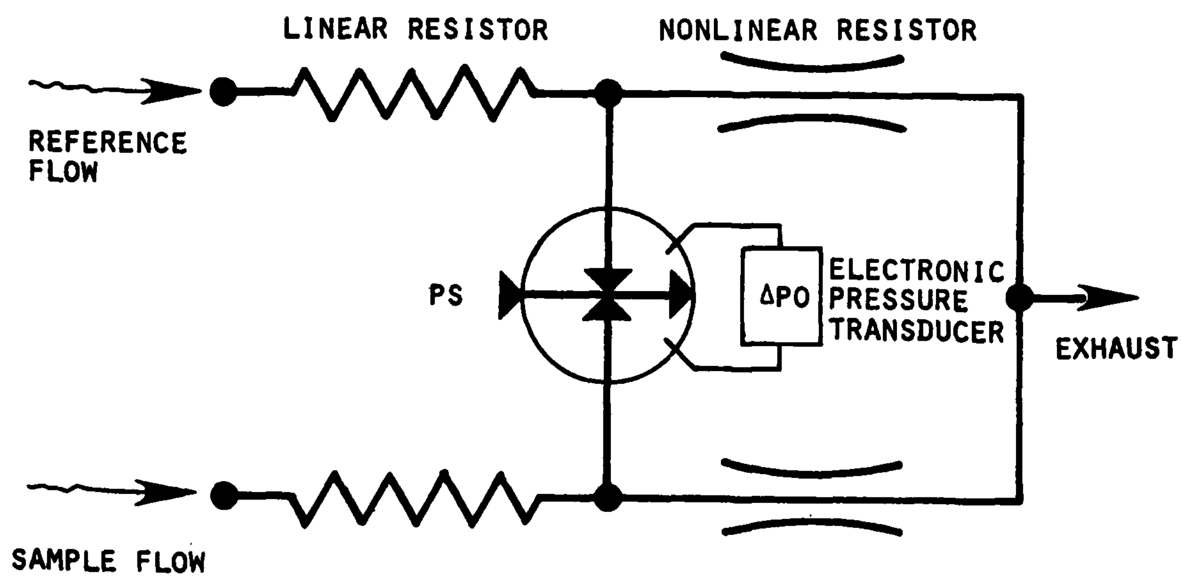

Figure 2. Resistor bridge schematic

A nonideal resistor contains both linear and nonlinear components. This can be written as

$$P = a\mu Q + b\rho Q^2 = AQ + BQ^2 \ . \tag{3}$$

Therefore, the pressure drop for a nonideal linear resistor is given by

$$P_L = A_L Q + B_L Q^2 \ . \tag{4}$$

For a nonideal nonlinear resistor, the pressure drop is

$$P_N = A_N Q + B_N Q^2 \ . \tag{5}$$

Once the A and B values for a resistor are known for one gas, they can easily be calculated for another gas. For example, if the value of B were desired for use in a second gas, B_2 could be calculated as follows:

$$B_2 = B_{AIR} \ \frac{\rho_2}{\rho_{AIR}} \ . \tag{6}$$

Similarly, the value of A_2 is given by

$$A_2 = A_{AIR} \ \frac{\mu_2}{\mu_{AIR}} \ . \tag{7}$$

For the bridge sensor, the second gas is the sample gas and is made up of a combination of two or more gases. The density of a gas mixture can be calculated using the linear relationship[1]

$$\rho_2 + \rho_a + \phi(\rho_b - \rho_a) \tag{8}$$

where

ϕ is the volume concentration of gas b in gas a and
2 refers to the gas mixture of gases a and b.

The viscosity of a gas mixture is a highly nonlinear function of the constituent gas viscosities:[2]

$$\frac{\mu_2}{\mu_a} = \frac{1}{1 + \frac{\phi}{1-\phi}\Psi_{ab}} + \frac{\frac{\mu_b}{\mu_a}}{1 + \frac{1-\phi}{\phi}\Psi_{ba}} \ , \tag{9}$$

where

$$\Psi_{ij} = \frac{1}{\sqrt{8}} \left[1 + \frac{M_i}{M_j}\right]^{-\frac{1}{2}} \left[1 + \left(\frac{\mu_i}{\mu_j}\right)^{\frac{1}{2}} \left(\frac{M_j}{M_i}\right)^{\frac{1}{4}}\right]^2 \ . \tag{10}$$

---

1 Joyce, James W., and Woods, Robert L., "Fluidic Sensors for Life Support Systems," Harry Diamond Laboratories, HDL-TM-75-17, October 1975.

2 Wilke, C.R., "A Viscosity Equation for Gas Mixture," J. Chem. Phys., Vol. 18, No. 4, pp. 517-519, 1950.

The resistor bridge was fabricated with TRITEC's etched 300 series stainless steel resistor laminates as shown in Figure 3. The pressure versus flow characteristics of these resistors in air were evaluated. A summary of both dimensional and performance data for these resistors is presented in Table III. Based upon calculated bridge performance and preliminary signal noise test results, the bridge chosen for extensive system testing consisted of the 3N3L resistor combination, i.e., the LR-3 linear resistor (0.11 mm thick) and the OR-3 nonlinear resistor (0.21 mm thick).

The sensitivity of the bridge was experimentally determined. Pure N_2 gas flowed through one side of the bridge and a calibrated gas mixture of CO_2 in N_2 flowed through the other. The output differential pressure signal for the bridge was noted for various combinations of bridge pressure (P_b) and CO_2 concentration for three different bridge designs.

In Figure 4, the experimental results for 5020 ppm CO_2 in N_2 (calibrated bottled gas mixture) are compared to theoretical predictions based on equations 4 through 10. System noise measurements are also presented in Figure 4. These data show that sensor signal short-term noise level is fairly independent of P_b until the sensor flow begins the transition to turbulence (P_b in the region of 55 to 60 mmHg). In addition to the short-term noise measured here, signal instability occurs in the form of random output signal null shifts as the turbulent flow region is approached. It was to avoid this instability that the operating pressure of the bridge was chosen as 42.5 mmHg, even though in terms of signal sensitivity and short-term noise level, a much greater signal resolution can be obtained at higher values of P_b.

The resolution of the bridge sensor to CO_2 in N_2 at $P_b = 42.5$ mmHg is defined as the gas concentration level at which output signal is equivalent to noise. This is seen to be 120 ppm CO_2 in N_2. This is equivalent to 111 ppm H_2S in air (for sensing H_2S) and 112 ppm CO_2 in Section 4). Compared to the calculated value of 2.9×10^{-6} mmHg/ppm CO_2 in N_2, the bridge signal level is somewhat less sensitive than expected. Measured sensitivity was found to be 9.0×10^{-7} mmHg/ppm CO_2 in N_2.

All pressure measurements taken during the evaluation of the resistor bridge were made with a Datametric barocel pressure sensor and all flow measurements were made with a National Instruments Laboratory Vol-O-Flo flow meter.

2.2 Vortex

The vortex sensor provides a signal that is directly proportional to the difference in densities between the reference and sample gas mixtures. The two flow streams are introduced on either side of a circular vortex chamber whose axis of symmetry is perpendicular to the gravitational field. This field creates a body force which acts on the two gases such that the lighter gas flows toward the top of the chamber as the flow exits through the center of the end wall of the chamber.

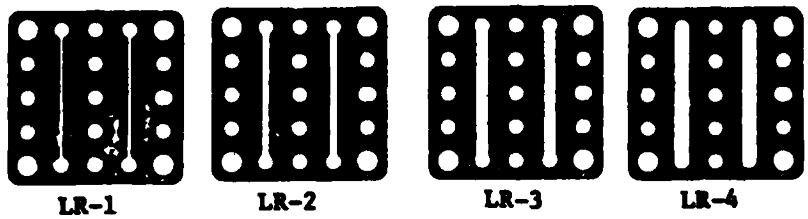

LINEAR RESISTOR LAMINATES

<u>LINEAR RESISTOR CHANNEL-WIDTH</u>

LR-1	0.64 mm
LR-2	1.27 mm
LR-3	1.91 mm
LR-4	2.39 mm

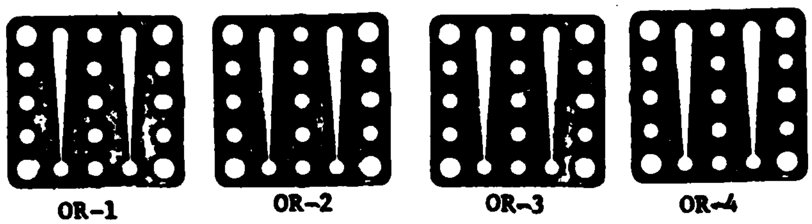

NONLINEAR (ORIFICE) RESISTOR LAMINATES

<u>NONLINEAR RESISTOR ORIFICE WIDTH</u>

OR-1	0.25 mm
OR-2	0.38 mm
OR-3	0.51 mm
OR-4	0.64 mm

Figure 3. Resistor bridge laminates

SYMBOL	BRIDGE SENSOR	DATA
□	#3N4L	CALCULATED VALUES FOR 5020 ppm CO_2 IN N_2
△	#2N4L	
○	#3N3L	
◧	#3N4L	EXPERIMENTAL VALUES FOR 5020 ppm CO_2 IN N_2
◭	#2N4L	
◐	#3N3L	
■	#3N4L	SENSOR NOISE LEVEL FOR PURE N_2
▲	#2N4L	
●	#3N3L	

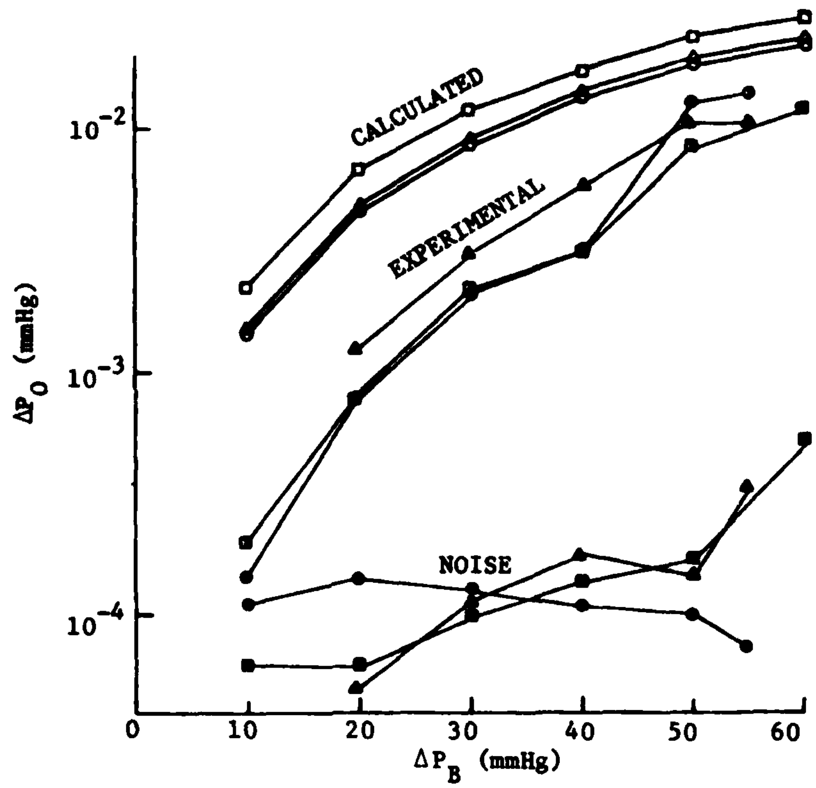

Figure 4. Bridge sensor signal and noise versus power supply

TABLE III. DIMENSIONAL AND PERFORMANCE DATA FOR BRIDGE SENSOR RESISTORS

NONLINEAR RESISTOR	OR-	ASPECT RATIO	W(mm)	d(mm)	A_N [illegible]/LPM	B_N [illegible]/$(LPM)^2$
1N	1	0.38	0.28	0.11	324.06	1133.79
2N	1	1.15	0.28	0.32	12.63	121.97
3N	2	0.52	0.40	0.21	16.76	202.16
4N	2	1.02	0.42	0.43	4.56	47.77
5N	3	0.60	0.53	0.32	1.39	47.18
6N	3	0.95	0.53	0.53	-5.63	17.93
7N	4	0.45	0.71	0.32	4.47	30.37
8N	4	0.90	0.71	0.64	0.09	8.90

LINEAR RESISTOR	LR-	ASPECT RATIO	W(mm)	d(mm)	L(mm)	A_L exp.	B_L exp.
1L	1	0.17	0.64	0.11	16.6	601.80	1109.66
2L	2	0.08	1.27	0.11	16.9	258.96	269.00
3L	3	0.06	1.91	0.11	17.5	199.37	134.00
4L	4	0.05	2.39	0.11	19.1	152.44	82.18

The strength of the vortex is proportional to the difference in gas densities. The vortex sensor is shown schematically in Figure 5. Note that for proper alignment of the sensor inlets and vortex chamber with the gravity field, the plane "g" must be perpendicular to the sensor's planar section that is shown in Figure 6.

The end wall of the vortex chamber contains the drain and the pickoff body. The pickoff body contains a sensor or pickoff that measures the strength of the vortex field in the chamber and provides a differential pressure that is proportional to that vortex strength. That signal can be measured directly by electronics or fluidically amplified to provide a convenient high-level pressure signal that is proportional to the concentration of the gas of interest in the sample gas stream.

The problem with accurate noise measurement is related to a design feature of the vortex sensor that limits its usefulness at this time. That limitation is the high impedance associated with the sensor's output signal. This high impedance makes the fluidic amplification of that signal very difficult. Therefore, even though the sensor may be able to resolve extremely low gas concentration levels, its usefulness is limited by the capabilities of the available pressure transducers. In addition, these transducers (with a resolution of about 10^{-6}mmHg) would add significantly to sensor system cost and decrease system reliability. If further development of the sensor improves the pickoff region so that fluidic signal amplification can be achieved, this sensor may become capable of providing inexpensive monitoring of gas concentration levels in ranges as low as 50 ppm.

An expression for the output signal can be written as

$$\Delta P = K(\rho_R - \rho_s) \quad , \tag{11}$$

where

ΔP = output differential pressure,

K = a proportionality constant,

ρ = gas density,

subscript R refers to the reference gas stream, and

subscript s refers to the sample gas stream.

The vortex sensor was fabricated from aluminum. That material was chosen because this was the only sensor that required extensive machining in the fabrication process. (Laminates for the resistor bridge and oscillators were chemically etched.) If this sensor is improved so that it adequately senses H_2S, it could also be fabricated from a stainless steel.

Preliminary testing included measurements of sensor flow rate versus supply pressure and null shift. These data are presented in Figures 7 and 8, respectively. Figure 8 also shows that signal noise level data averages about 8×10^{-7}mmHg. It should be noted that this

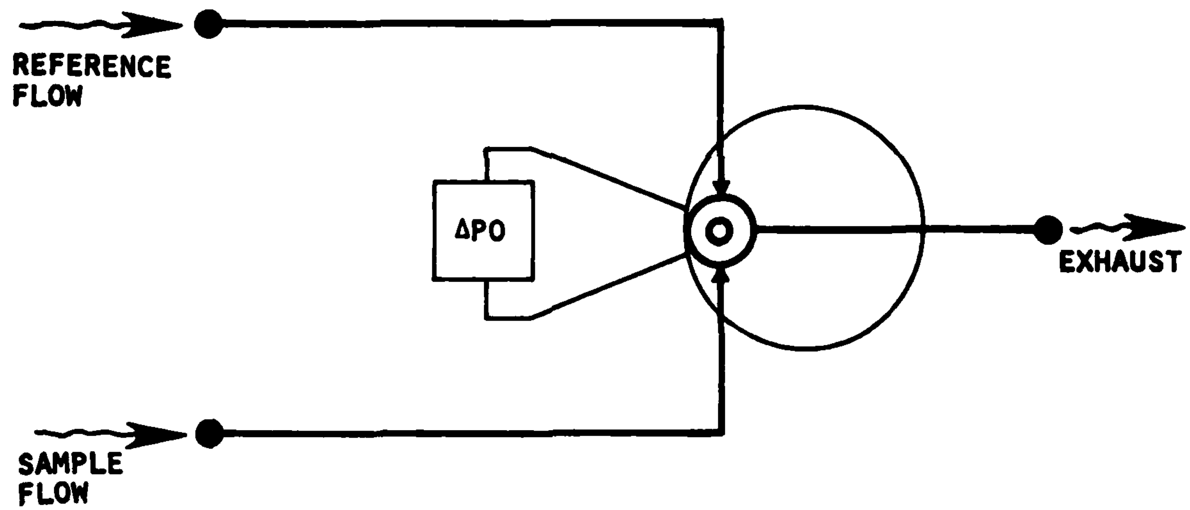

Figure 5. Vortex sensor schematic

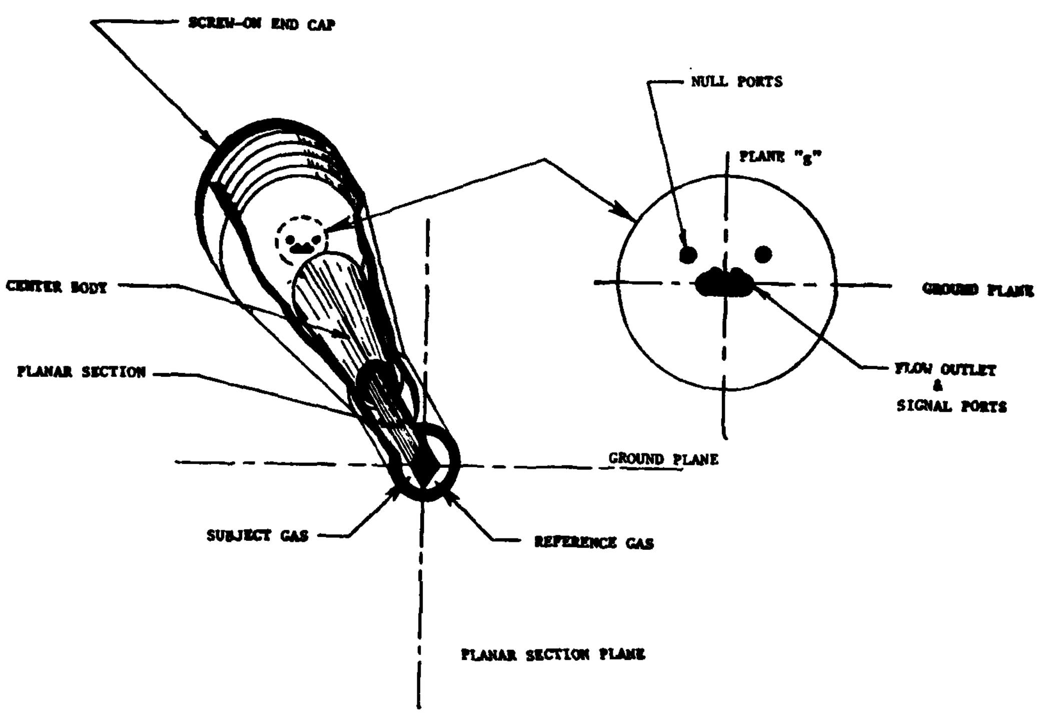

Figure 6. Vortex sensor planar section.

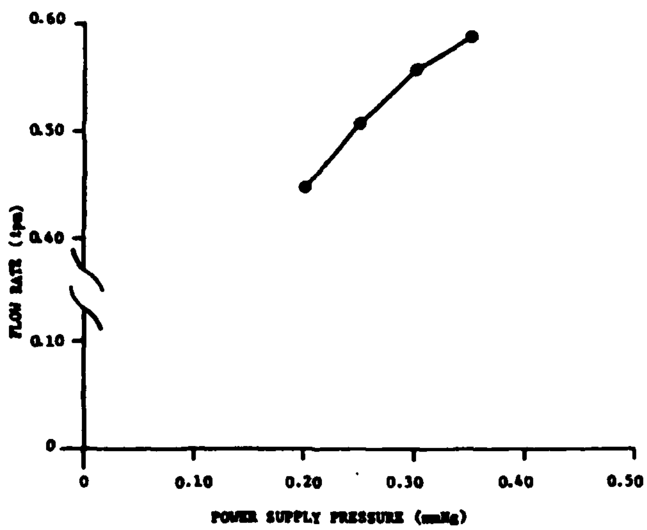

Figure 7. Vortex sensor flow rate versus supply pressure

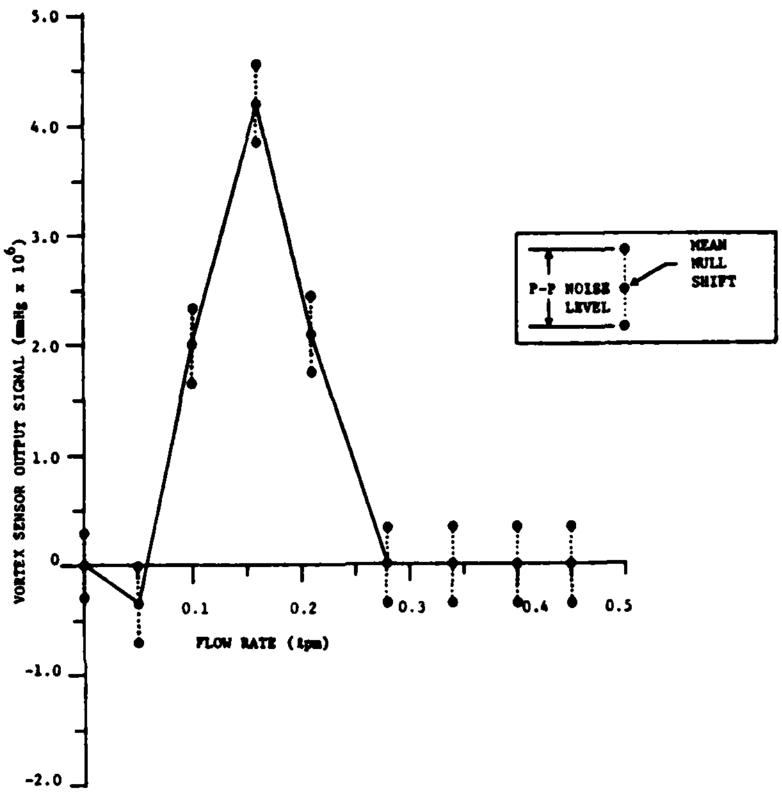

Figure 8. Vortex sensor flow rate versus null shift and noise.

noise is a function of both the sensor and the pressure transducer as its source. Since the measured noise level corresponds to the noise level of the transducer alone, it can only be assumed that sensor noise is no greater than that of the transducer.

The sensitivity of the vortex sensor was experimentally determined. Using N_2-in-air gas mixtures, the value of K in equation 11 was found to be 116 mmHg-cm^3/g. This is equivalent to a sensitivity of 7.3 x 10^{-8} mmHg/ ppm of CO_2 in air and 2.5 x 10^{-8} mmHg/ppm of H_2S in air.

2.3 Oscillator

The jet edge resonator oscillator is essentially a whistle. In its simplest form, it consists of a power jet flowing past a cavity and impinging upon an edge. Impingement upon the edge causes vortex shedding by the jet. The vortex shedding causes pressure fluctuations on either side of the jet. The frequency of the fluctuations has been empirically determined and is given by [3]

$$f_e = 0.466j \frac{u}{h} , \tag{12}$$

where

f_e = edgetone frequency ,

u = jet velocity ,

h = distance the jet travels before encountering the edge, and

j = 1.0, 2.3, 3.8, or 5.6 .

Relatively high amplitude pressure fluctuations (10^{-3} mmHg or more) are obtained when the edgetone frequency is equal to the resonant frequency of the cavity. This frequency is given by

$$\bar{f} = K_a , \tag{13}$$

where

$\bar{f}$ = oscillator mean frequency ,

K = a constant, a function of cavity geometry and supply pressure ,

a = $\sqrt{\gamma RT}$, the speed of sound in the gas ,

γ = c_p/c_v, the ratio of specific heats ,

c_p = gas specific heat at constant pressure ,

c_v = gas specific heat at constant volume ,

3 Gaylord, Wilmer and Carter, Vondell, "Fluerics 27. Flueric Temperature Sensing Oscillator Design," Harry Diamond Laboratories HDL-TR-1428, April 1969.

$R = 8314/M$ (m^2/s^2 - ^{o}K), the universal gas constant,

M = molecular weight of the gas, and

T = absolute temperature (K) of the gas.

Since the frequency signal of this device is a function of the gas properties c_p, c_v, and M, it can be used as a gas concentration sensor. Based upon equation 13 an expression for oscillator sensitivity has been developed.[4]

$$\frac{\bar{f}_S}{\bar{f}_R} - 1 = \left[\frac{\frac{1}{\phi}\left(\frac{1}{\phi} + \frac{M_1}{M_R}\,\frac{c_{p1}}{c_{pR}} - 1\right)}{\left(\frac{1}{\phi} + \frac{M_1}{M_R} - 1\right)\left(\frac{1}{\phi} + \frac{M_1}{M_R}\,\frac{c_{v1}}{c_{vR}} - 1\right)}\right]^{1/2} - 1 \qquad (14)$$

where

ϕ = volume concentration in the sample gas of the gas to be sensed,

subscript S refers to the sample gas,

subscript R refers to the reference gas, and

subscript 1 refers to the gas to be sensed.

This expression assumes that the temperatures of the two gas streams and the constant K for the two oscillators are equal. If this is not the case, the equation is

$$\frac{\bar{f}_S}{\bar{f}_R} - 1 = \left[\frac{\frac{1}{\phi}\left(\frac{1}{\phi} + \frac{M_1}{M_R}\,\frac{c_{p1}}{c_{pR}} - 1\right)}{\left(\frac{1}{\phi} + \frac{M_1}{M_R} - 1\right)\left(\frac{1}{\phi} + \frac{M_1}{M_R}\,\frac{c_{v1}}{c_{vR}} - 1\right)}\,\frac{T_S}{T_R}\right]^{1/2} \frac{K_S}{K_R} - 1. \qquad (15)$$

Processing the frequency ratio signal is most easily accomplished with a counter circuit. The two oscillator's signal cycles are accumulated in counters until the first counter (for f_R) reaches a predetermined count (n_R), at which time the second counter (for f_S) stops counting. The count in the second counter (n_S) can be used as the system signal. This is demonstrated as follows:

$$\frac{f_S}{f_R} = \frac{f_S t}{f_R t} = \frac{\left(n_S + \frac{1}{2}\right) \pm \frac{1}{2}}{n_R}\,, \qquad (16)$$

4 Villarroel, Fernando, and Joyce, James W., "Flueric Carbon Dioxide Concentration Sensor," ASME Paper No. 70-WA/Flcs-10, November 1970.

where t is the time over which the signal cycles are counted. Since the predetermined value of n_R is known, the value of n_S determines the value of $f_S/f_R - 1$, the system signal. This measurement system is shown schematically in Figure 9.

Several sources of error arise when this type of scheme is used. These include instabilities or jitter in the oscillators, temperature differences in the gas stream, trigger error in the counter circuits, and counter roundoff error of $\pm$ 1/2 cycle of the sample gas frequency signal. The frequency signal noise (jitter), or deviation of the frequency signal from the mean frequency can be expressed as follows:

$$J = \left| f - \bar{f} \right| = C/\sqrt{n} = C/\sqrt{ft} , \tag{17}$$

where

J = signal noise ,

f = the frequency of the oscillator signal measured over time, t ,

C = a function of oscillator design geometry and power supply pressure ,

n = the number of signal cycles over which the frequency is averaged , and

t = the time over which the frequency is averaged.

For $\phi = 0$, assuming no gas stream temperature differences, a trigger error of no greater than 0.02 cycle, and that $K_S = K_R$, then the maximum frequency ratio signal measurement error (E) can be written as:

$$E = \frac{\bar{f}_S + J_S + (1/2 - \text{count error})}{\bar{f}_R - J_R - (\text{trigger error})} - \frac{\bar{f}_S}{\bar{f}_R} = \frac{n_S + C\sqrt{\frac{t}{\bar{f}}} + 1/2 + 0.02}{n_R - C\sqrt{\frac{t}{\bar{f}_R}} - 0.02} - \frac{\bar{f}_S}{\bar{f}_R} \tag{18}$$

The general design of the oscillators evaluated during this effort is shown in Figure 10. Specific designs are implemented by combining the etched stainless steel laminates, shown in Figure 11. Two sizes of the oscillator were evaluated. These were designated OS-2 and OS-4. Laminates OS-1 and OS-3 were added to OS-2 and OS-4 laminates, respectively, to control the outlet-to-inlet nozzle area ratio and thus affect such sensor performance characteristics as oscillation supply pressure threshold and the dependence of frequency variation on variables of supply pressure. It is desirable to minimize supply pressure threshold to reduce sensor power consumption and depletion of the chemical processor. Minimization of frequency dependence on supply pressure reduces the

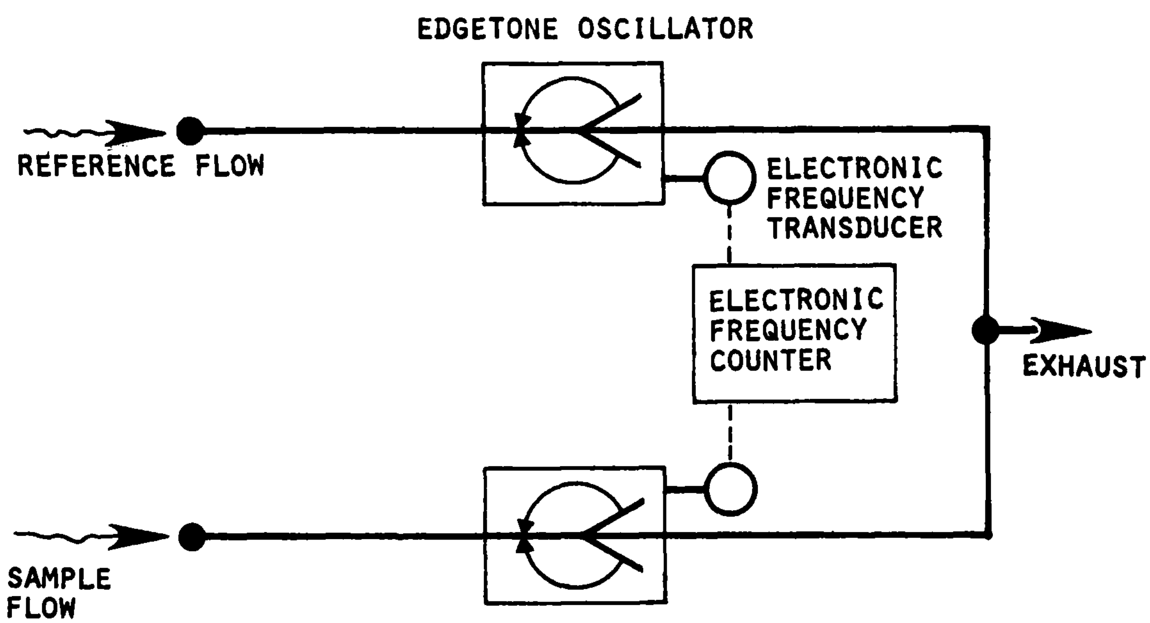

Figure 9. Oscillator sensor schematic

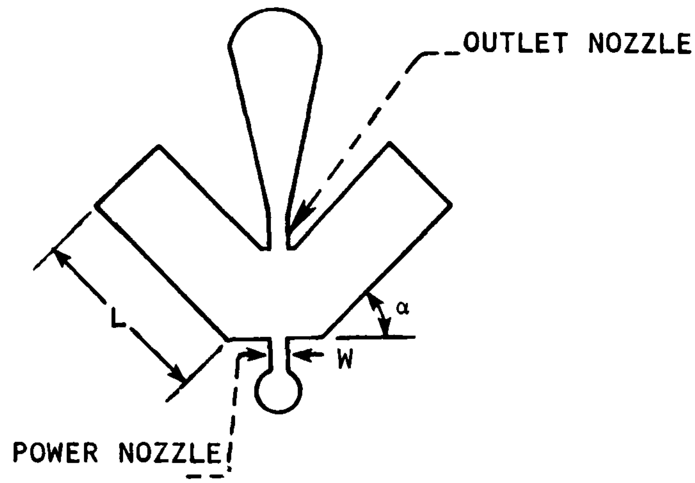

	OS-2	OS-4
L	8.41 mm	4.78 mm
W	1.19 mm	0.64 mm
h	3.99 mm	1.98 mm
α	45°	45°

Figure 10 Oscillator sensor design

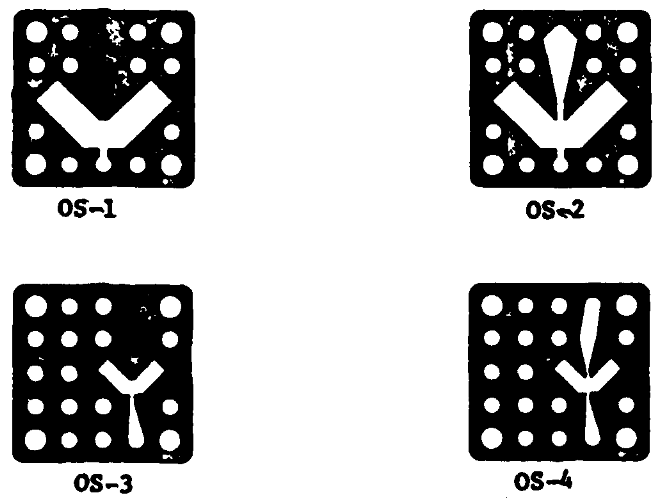

OSCILLATOR LAMINATES

OSCILLATOR	POWER NOZZLE-LENGTH, WIDTH
OS-2	2.39 mm, 1.19 mm
OS-4	1.19 mm, 0.64 mm

Figure 11. Oscillator sensor laminates

possibility of signal null shifts due to power supply pressure fluctuations.

Oscillators consisting of a number of combinations of OS-1, OS-2, and OS-3, OS-4 laminates were tested to determine an optimum design. Sensor threshold was monitored. The results of these tests are given in Figure 12.

Two oscillators each consisting of five OS-4 laminates (0.11 mm thick) were chosen for further testing. The sensors were manifolded together so that they shared common supply and outlet pressure as they would in the full sensor system. A vacuum was applied to their outlet ports and air was drawn through them. The frequency of one oscillator (f_A) and the flow required to drive it were recorded over a range of outlet pressure valves. Oscillation threshold occurred at 27 mmHg vacuum. Data were recorded for pressures down to 150 mmHg vacuum. Fifteen readings of frequency f_A and frequency ratio of the two oscillators were recorded at each outlet pressure. These readings were used to determine the value of C in equation 17, and to calculate the mean frequency ratio, as well as its standard deviation or noise. Figure 13 illustrates the data obtained from these sensors.

Evaluation of the data shows that, for the selected oscillators, the optimum operating point is for an outlet pressure of about 68 mmHg vacuum. This minimizes the signal (f_A/f_B) sensitivity to vacuum level, its standard deviation, and the flow required for sensor operation.

Figure 14 shows sensor-system noise level and required threshold, based on equations 15 and 18, for various signal sample times. A value of C = 36 for equation 18 was calculated from data of single-oscillator frequency stability, using equation 17.

Also shown in Figure 14 is the standard deviation of the system signal for 100 signal samples at several signal sample times. Agreement of data with equation 18 is quite good for signal sample times below 10 seconds. Data for the only signal sample time greater than 10 seconds (71 seconds) did not agree with the predicted trend. This is because of a gradual drift in power supply level over the time of the test (greater than 2 hours). However, even if this power supply drift problem were eliminated, this figure shows that the noise level is too large to permit resolution of 5 ppm H_2S in air for a reasonably short signal sample time.

Redesign of this sensor to include a smaller supply nozzle (to lower flow requirements) and smaller resonant cavities (to increase frequency and decrease required sample time) might improve sensor performance sufficiently (if the jitter constant C does not also increase) to fulfill the requirements of the offshore application. Since such redesign was beyond the scope of this effort, no further tests were conducted on this type of sensor.

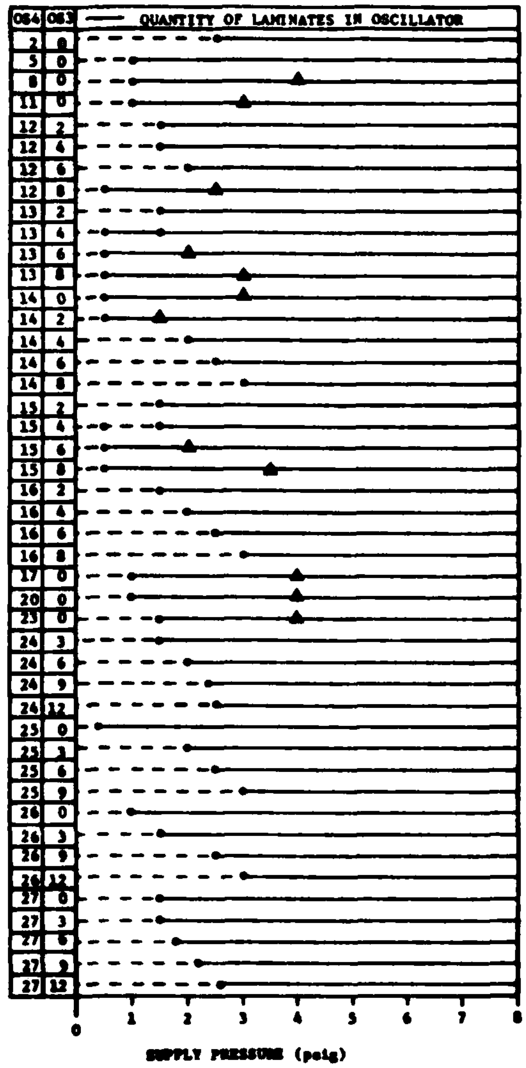

- - - random oscillation

—— sinusoidal oscillation

-●- transition point

-▲- frequency jump

Figure 12. Oscillator sensor threshold data

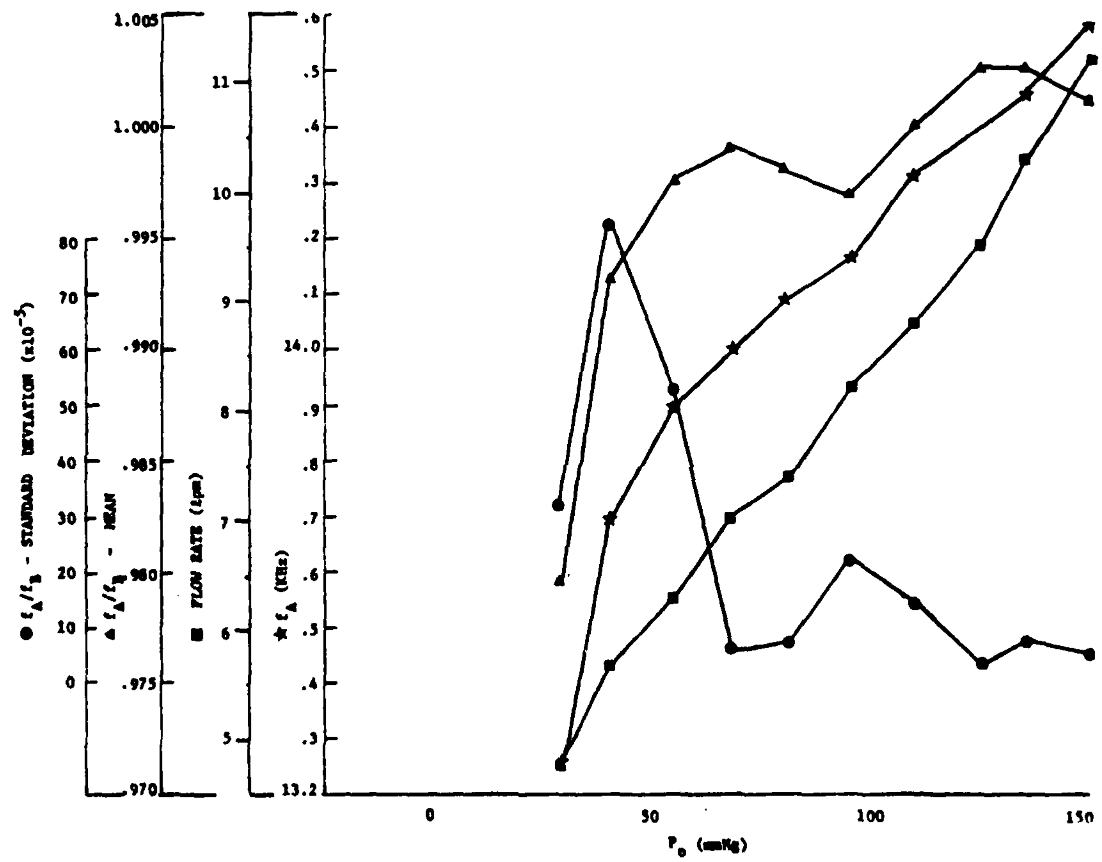

Figure 13. Oscillator sensor performance characteristics

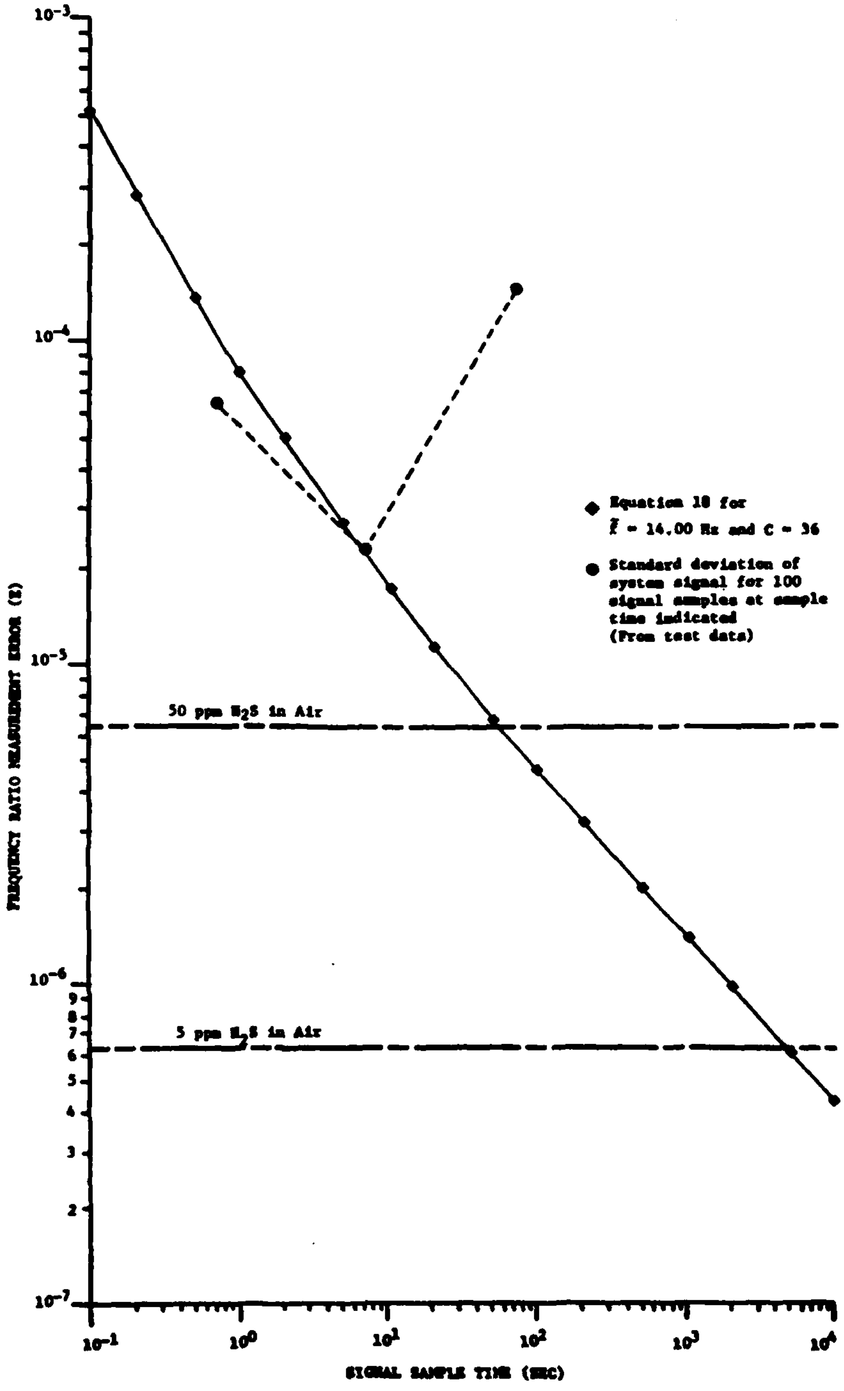

Figure 14. Oscillator sensor-system noise level and theoretical threshold of H_2S in air.

3. HEAT EXCHANGER

All three fluidic sensors are sensitive to any temperature differential in the two (sample and reference) gas streams. The chemical processor for the hydrocarbon-sensing system must be heated (see Section 4), thus increasing the possibility of nonuniform temperature in the two gas streams. To eliminate this problem, a heat exchanger for the two gas streams was placed between the chemical processor and the fluidic sensor.

Heat exchanger laminates are shown in Figure 15. Laminate HE-1 contains the snake-like channel (HE-1). The basic heat exchanger unit (a flow path module) is constructed by stacking the laminates in the order shown in Figure 16.

The module forms two separate gas flow paths (sample and reference) which are aligned to share maximum membrane area. Heat from the high temperature gas stream flowing through the channel plates is transferred to the membrane plate (HE-2) and from there to the low temperature gas stream, thus lowering the differential temperature between the two flow paths. The efficiency of the heat exchanger increases with increasing membrane area shared between the flow paths.

The basic heat exchanger is made up of a number of flow path modules combined in parallel so that an equal amount of flow passes through each module. Each flow path has two inlets and two outlets on each end of the stack, one set each for the sample and reference flow paths. Figure 17 is a schematic of the heat exchanger assembly that is used with the resistance bridge sensor.

The heat exchanger constructed for this program contains seven of the flow path modules shown in Figure 16. Tests were conducted to evaluate its ability to equalize temperature differential between two gas streams. With one gas stream held at room temperature, the other gas stream was heated in an oven. The input and output differential temperatures of the gas streams were recorded as the heated stream temperature was increased from room temperature to more than 175°C. This test was conducted with equal channel flow rates of 3 and 5 ℓpm per channel. The test data are shown in Figure 18. These data were used to calculate the ratio of differential temperature into the heat exchanger to differential temperature out. This is shown in Figure 19.

The results of the tests show that small temperature differences (less than 50°C) should be reduced to less than 0.02°C (temperature monitoring equipment accuracy) at the heat exchanger outlet. In addition, small temperature differences are reduced by a factor of at least 2,000 for a 3 standard ℓpm flow in each channel and by 2,000 for a 5 standard ℓpm flow rate (see Figure 19). Heat exchanger efficiency (temperature difference reduction ratio) below T_{IN} = 130°C increases with decreasing flow rate. These results are very compatible with gas sensor system requirements since the gas stream temperature difference at the inlet to the heat exchanger is expected to be no more than 5°C. In addition, flow rates through the bridge sensor are 0.15 ℓpm per channel, much less than those present in the heat exchanger during this evaluation.

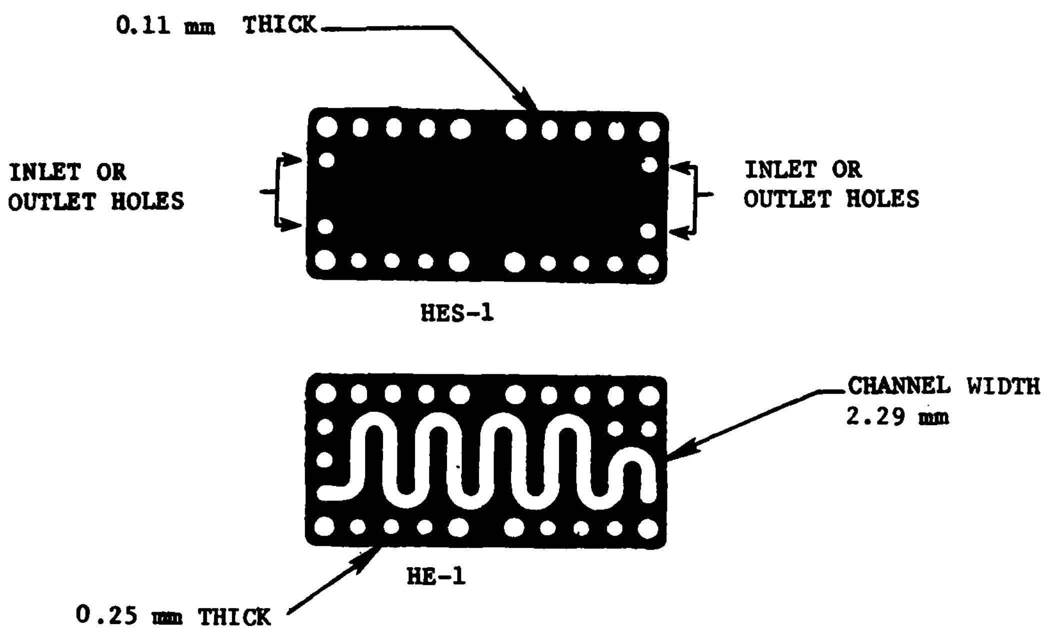

Figure 15. Heat exchanger laminates

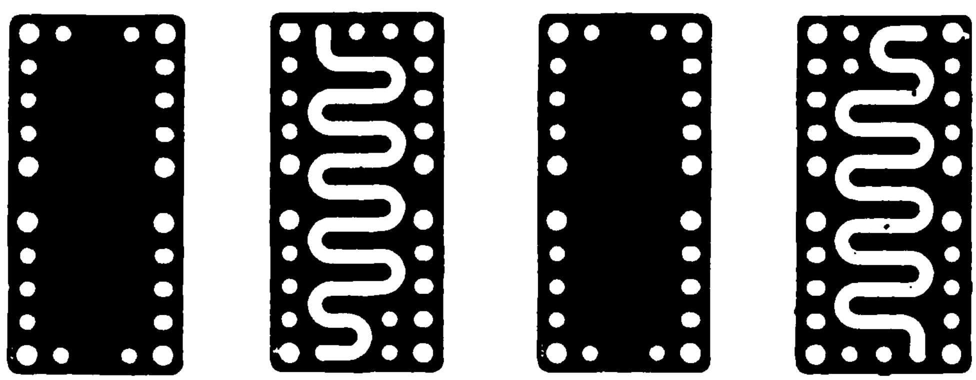

Figure 16. Stacking order of heat exchanger

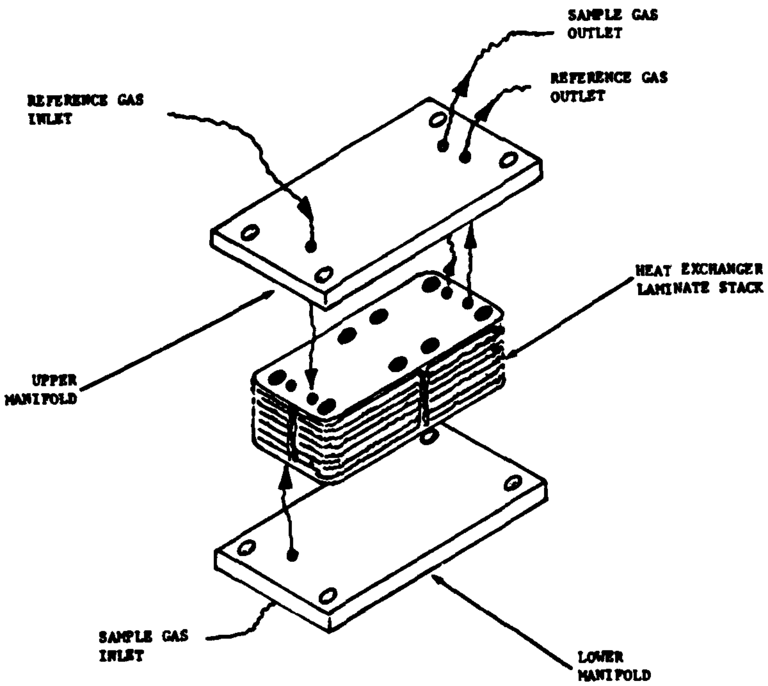

Figure 17. Heat exchanger assembly schematic

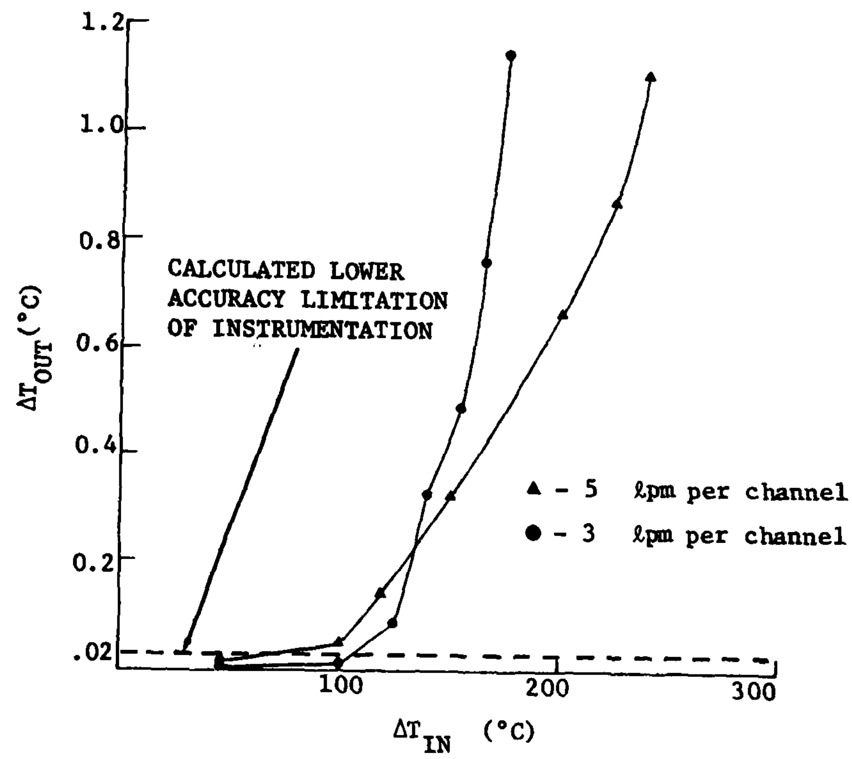

FIGURE 18. Differential-temperature reduction data for heat exchanger

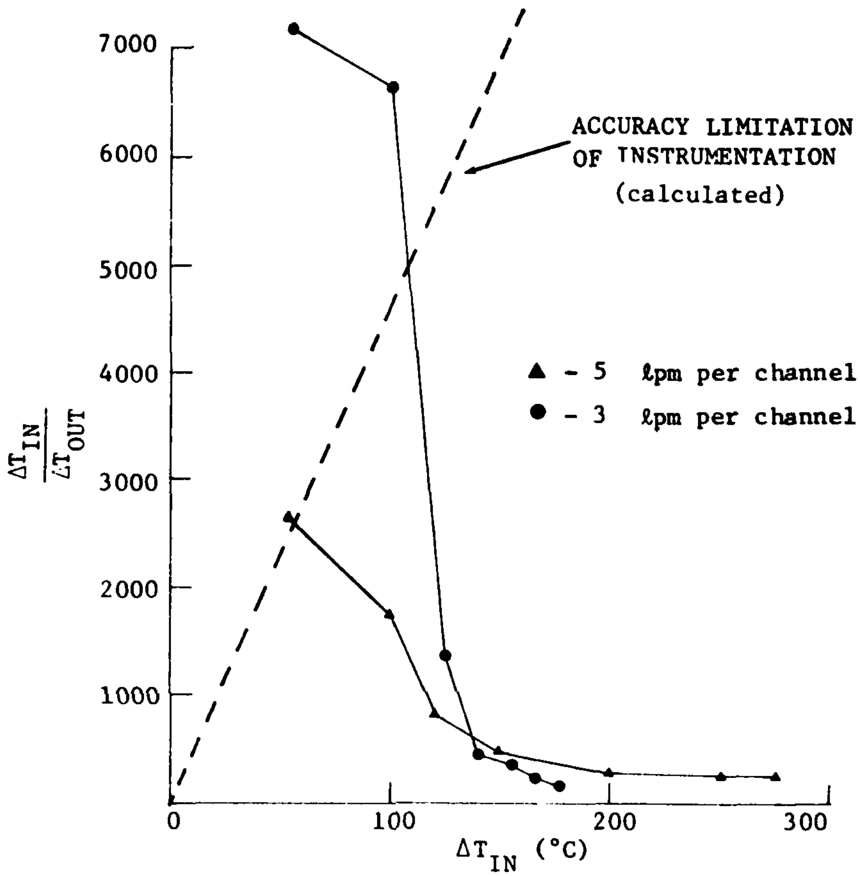

Figure 19. Differential temperature-reduction ratio data for heat exchanger

Referring to Table II, a temperature difference of about 0.3°C corresponds to a 1000 ppm H_2S in air signal in the resistor bridge sensor system. Therefore, the sensor system should be immune to temperature differences generated in a chemical processor.

4. CHEMICAL PROCESSORS

The function of the chemical processors is to change bulk gas mixture properties (density, viscosity, etc) in direct proportion to the concentration of the gas to be sensed. The processor must be specific to the subject gas (i.e., no other gas present is affected by the processor). The selection of the chemical processors evaluated during this effort was based on a chemical analysis,[5] the availability of the chemical required, and the cost of the processors.

For the hydrogen sulfide sensor system, the chemical processor housing contains metal-salt flakes mixed with an inert filler (see Figure 20). Two metal salts (lead acetate and silver nitrate) were evaluated. Chemical processors using these salts change the bulk gas properties of a hydrogen sulfide gas mixture by removing the hydrogen sulfide from the mixture. The hydrogen sulfide reacts with the metal-salt. The resultant sulfur compound remains on the metal-salt flakes. The reactions for the two metal-salts are given by

$$H_2S + 2AgNO_3 \longrightarrow Ag_2S + 2HNO_3 + 26.7\ \text{kcal/mol} \tag{19}$$

and

$$H_2S + Pb\,(OAc)_2 \longrightarrow PbS + 2HOAc + 200\ \text{kcal/mol}\ . \tag{20}$$

A problem had originally been anticipated with moisture being absorbed by metal-salt powders. This could cause the powders to stick together, thereby decreasing the available reactant surface area and the efficiency of the hydrogen-sulfide conversion. This problem was avoided by using the metal-salt flakes rather than powder and separating the flakes with fine washed sand (inert filler).

Two sets of tests to determine the conversion efficiency (reduction in H_2S concentration) of the metal-salt processors were conducted. The first used 25% metal-salt and 75% washed sand, while the second used 75% metal salt and 25% washed sand.

A calibrated gas mixture of 48.7 ppm H_2S in N_2 flowed through the processors at 1.4 ℓpm while gas samples were taken at the inlet and outlet. The samples were evaluated for H_2S content on a gas chromatograph with a flame photometric detector that had an accuracy of $\pm$ 0.01 ppm H_2S.

---

5 Ostdiek, A.J., "Fluidic Sensors for the Detection of Hydrogen Sulfide Gas and Natural Gas," Report #121, NEOS, Inc., May 1977.

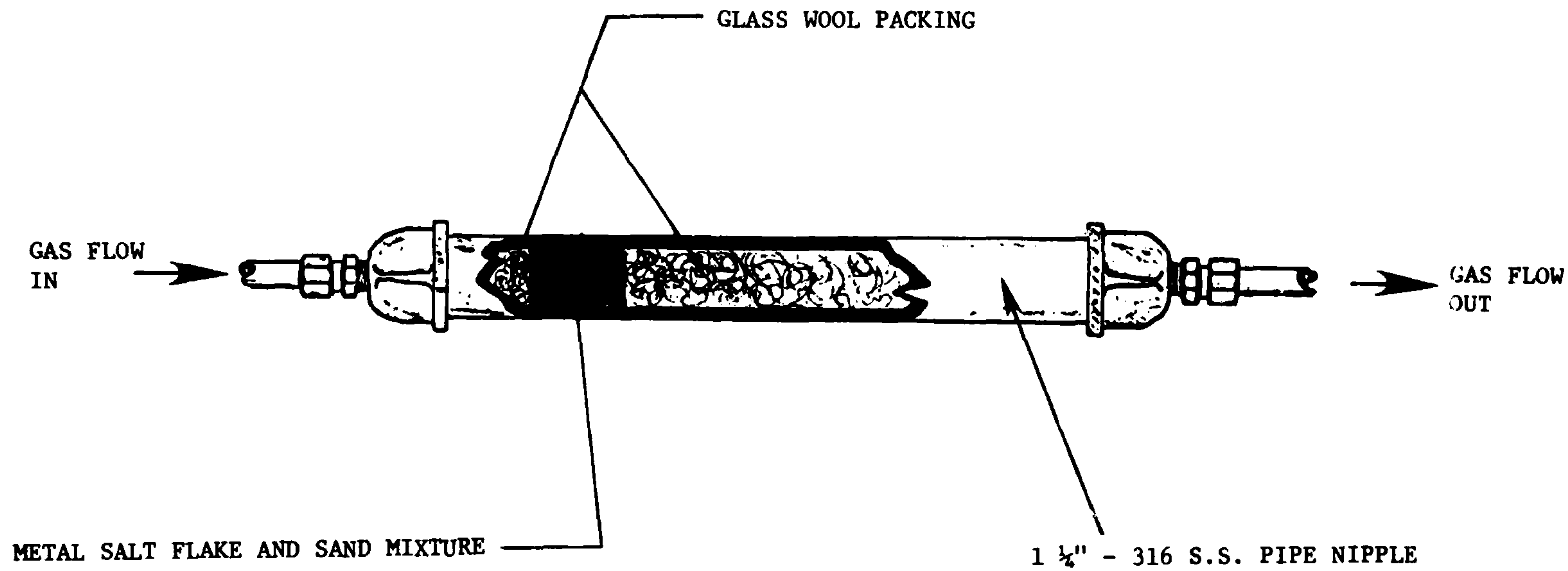

Figure 20. Metal-salt chemical processor housing

The H_2S in N_2 mixture was run through each processor for one hour and then room air was drawn through them at 1.4 ℓpm until the next hour long H_2S injection. Time histories of these tests are shown in Figure 21. Because of the relatively low conversion efficiency of both the 25% metal-salt, 75% washed-sand processors, testing was discontinued after the first few injections of H_2S.

Better results were obtained for the 75% metal-salt, 25% washed-sand processors. While the silver nitrate processor was unable to retain 100% conversion efficiency over a one hour H_2S injection, the lead acetate processor was able to run without any detectable signal reduction during four separate hour long injections. These results are also illustrated in Figure 21.

The lead acetate flakes are larger than those of silver nitrate, thus there is a difference in surface area per unit volume. Therefore, a smaller volume of silver nitrate than lead acetate was used to facilitate evaluation of the processors on an equal surface area basis (75 cm^3 for silver nitrate mixture versus 100 cm^3 for lead-acetate mixture). The lead-acetate processor out-performed the silver-nitrate processor as described above. In addition, silver nitrate costs $20.00/oz.* while lead acetate costs $0.50/oz. Therefore, the lead acetate processor (75% lead-acetate, 25% washed sand) was chosen for use in the H_2S sensor system.

The chemical processor for the hydrocarbon-sensor system uses the principle of catalytic conversion. The bed of the hydrocarbon processor is composed of alumina pellets covered with a thin coating of the catalyst. Figure 22 is a photograph of these commercially available pellets.

Two different catalyst coatings (platinum and palladium) were evaluated. Both types were developed for use by the auto industry to reduce exhaust gas hydrocarbon emissions. Both have a long life (more than a year) when used for this purpose. Suppliers of this catalyst material could only provide a rough idea of the quantity of catalyst beads required to meet the needs of the gas sensor system. Two housings were selected and filled with the recommended quantity of beads (see Figure 23). One was filled with platinum-coated beads and the other with palladium-coated beads.

A system was built to provide the required heat and temperature control for the palladium processor. The chemical processor and heating elements are enclosed in a 3 in. layer of alumina insulation. This is sufficient to keep the surface temperature of the insulation below 40°C when the interior of the chemical processor is 400°C. The original intention was to heat the reference gas stream as well as the sample gas stream flowing through the processor. This was done to decrease any possible degradation of the bridge sensor signal due to a differential temperature between the reference and sample gas streams. However, operating the catalytic chemical processor showed that heating was not required. While the interior of the processor is 400°C, temperature of the gas stream at the inlet and outlet

---

* June 1979 estimate

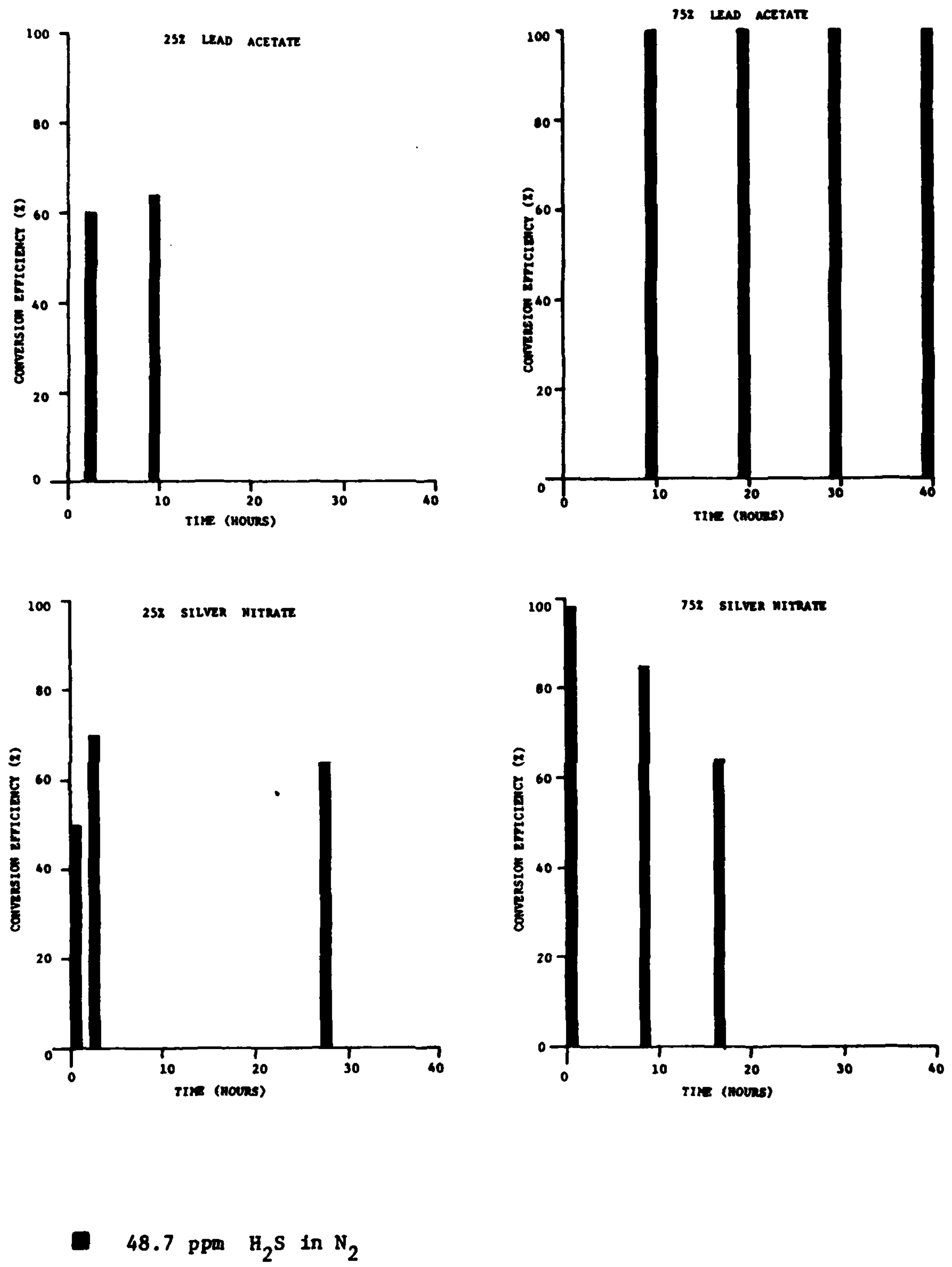

Figure 21. Efficiency of metal-salt chemical processor conversion versus time

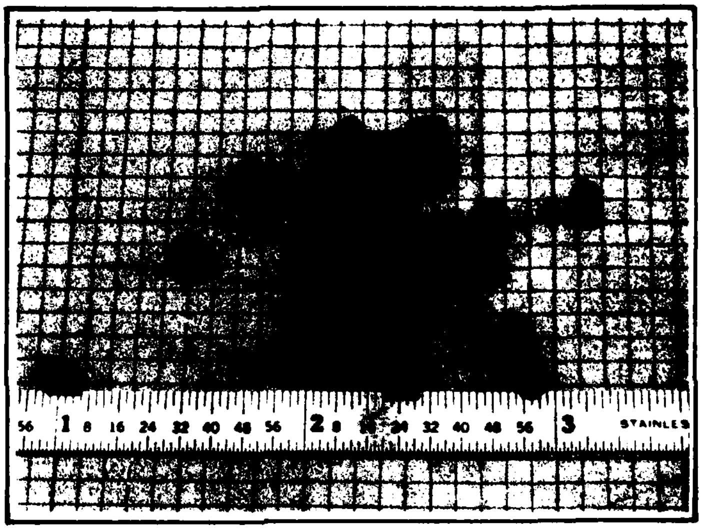

Figure 22. Catalyst pellets

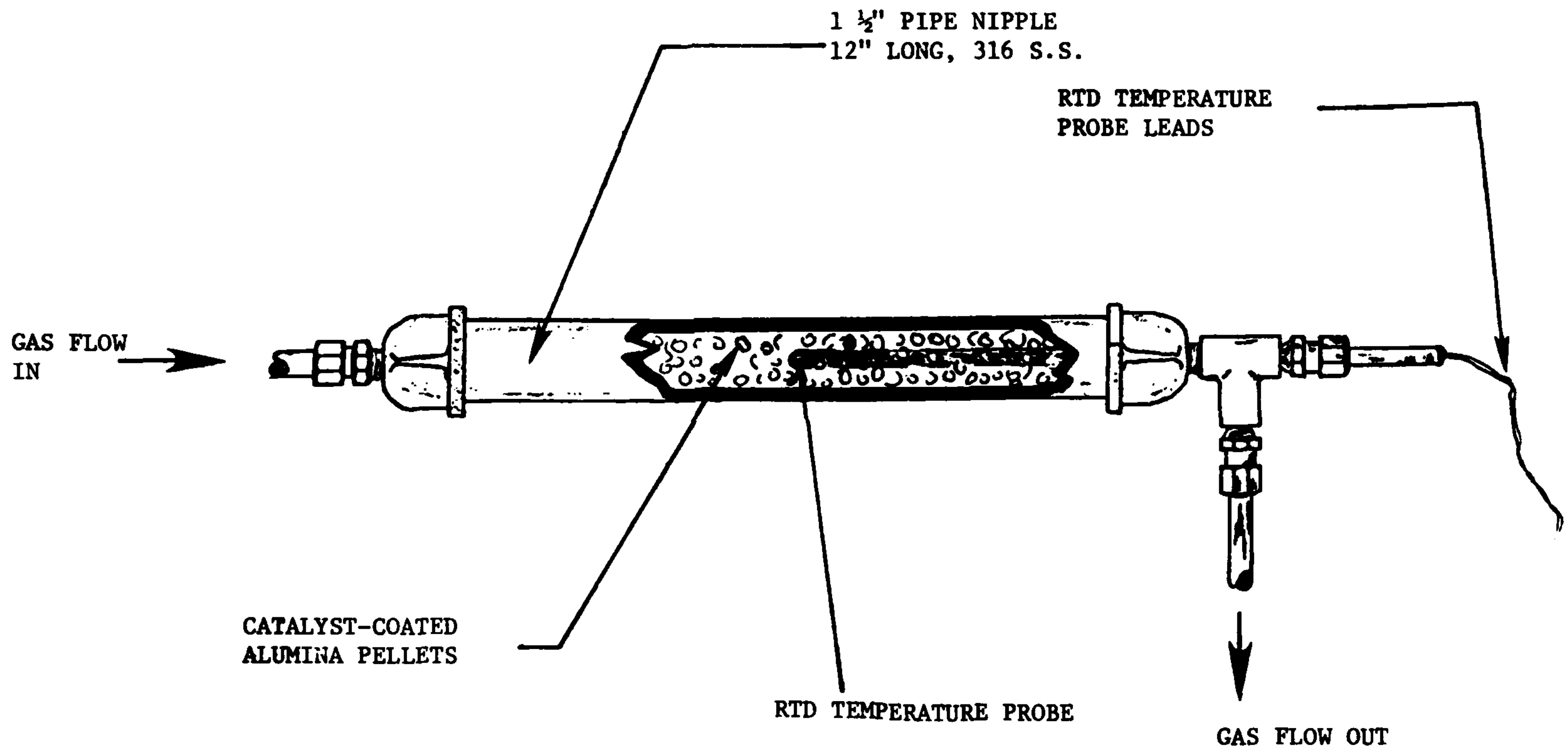

Figure 23. Catalyst chemical processor housing

remain at room temperature as close as 3 in. from the insulation. Therefore, for design simplicity, the reference flow path was left at room temperature.

With the entire gas sensor system assembled and running, thermocouple probes with a differential temperature resolution of 0.02°C were inserted in the reference and subject gas streams between the catalytic processor and the bridge sensor. No temperature difference between the two streams was observed.

The testing of the catalyst processors involves heating the processors to the recommended temperature (300° to 400°C for palladium and 500°C for platinum) and then flowing several concentrations of methane in air through them. Methane was chosen as the hydrocarbon gas for use in testing the processor performance since it is the most difficult of the hydrocarbons normally encountered offshore to catalytically oxidize. The reaction for methane is represented by

$$CH_4 + 2O_2 \xrightarrow{\text{Pd or Pt}} CO_2 + 2H_2O + 192 \text{ kcal/mole}$$

Because long catalyst life was established by the auto industry, this investigation concentrated on the efficiency of the processors. Efficiency is defined as the percentage of reduction effected in methane concentration. Efficiency was determined by taking gas samples at the inlet and outlet of the chemical processor and analyzing the gas makeup with a gas chromatograph equipped with a thermal conductivity sensor that has an accuracy of $\pm$100 ppm of methane in air. These data, in terms of conversion efficiency of the palladium catalyst, are shown in Figure 24.

Figure 24 shows that conversion efficiency increases with decreasing flow rate and decreasing methane concentration. Conversion efficiency at the flow rate required for the resistor bridge (0.15 ℓpm) is greater than 97%, regardless of temperature or concentration.

The cost for either the palladium or the platinum catalyst is about the same. Since, when used in conjunction with the resistor bridge, the palladium processor will have a conversion efficiency of nearly 100%, and since the operating temperature for the platinum processor is rated 100°C higher than that for the palladium processor, the platinum processor was not tested and the palladium processor was chosen for the hydrocarbon sensor system.

5. GAS SENSOR SYSTEM

5.1 System Design

Shown in Figure 25 is a schematic of the hydrocarbon gas sensing system. The chemical processor contains the palladium catalyst as described in Section 4. Gas density and viscosity changes in the reference gas stream are produced by hydrocarbon oxidation in the chemical processor. These gas mixture bulk property changes are detected by the fluidic resistor bridge sensor described in Section 2.1. The differential pressure signal

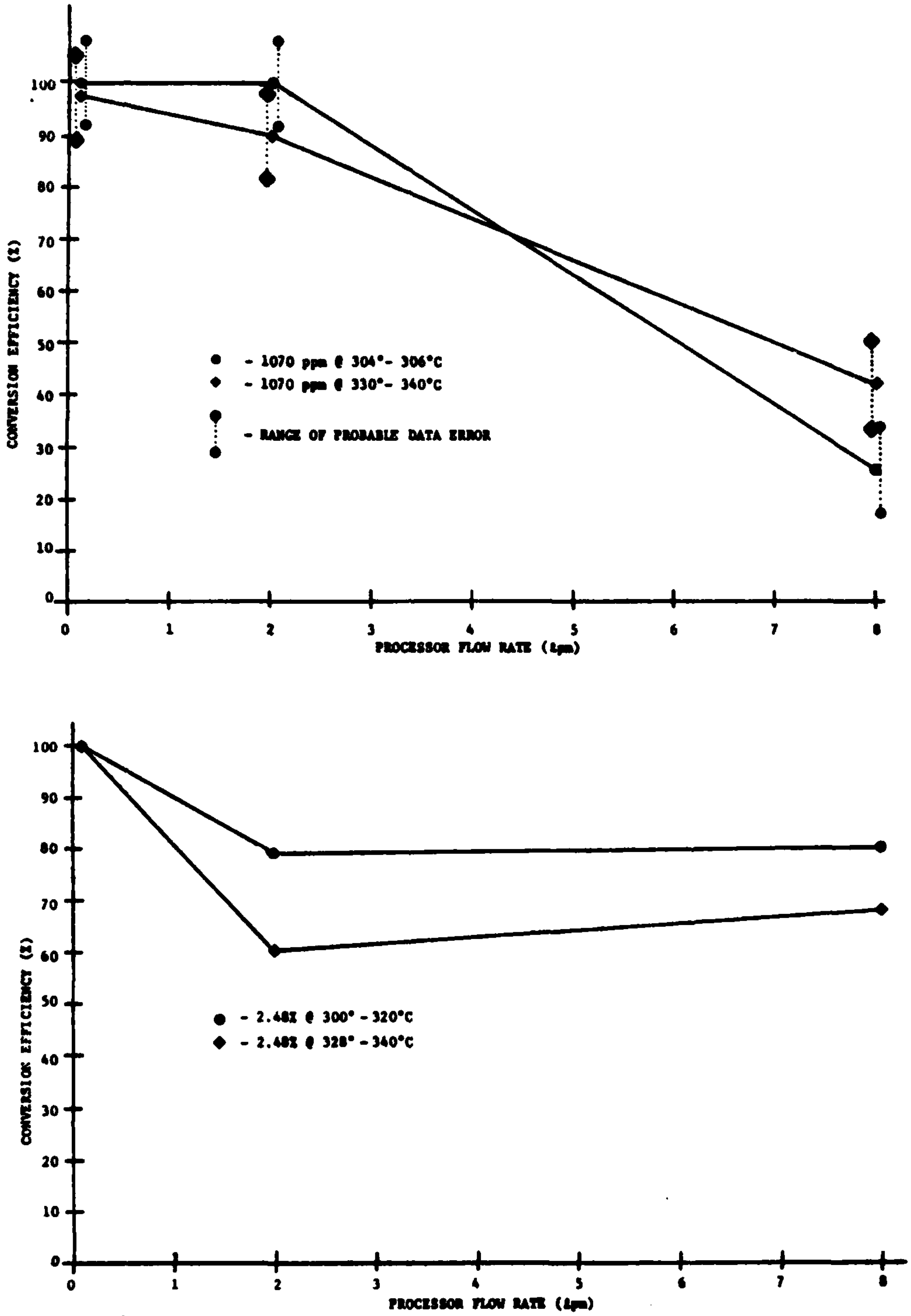

Figure 24. Methane reduction efficiency of palladium chemical processor

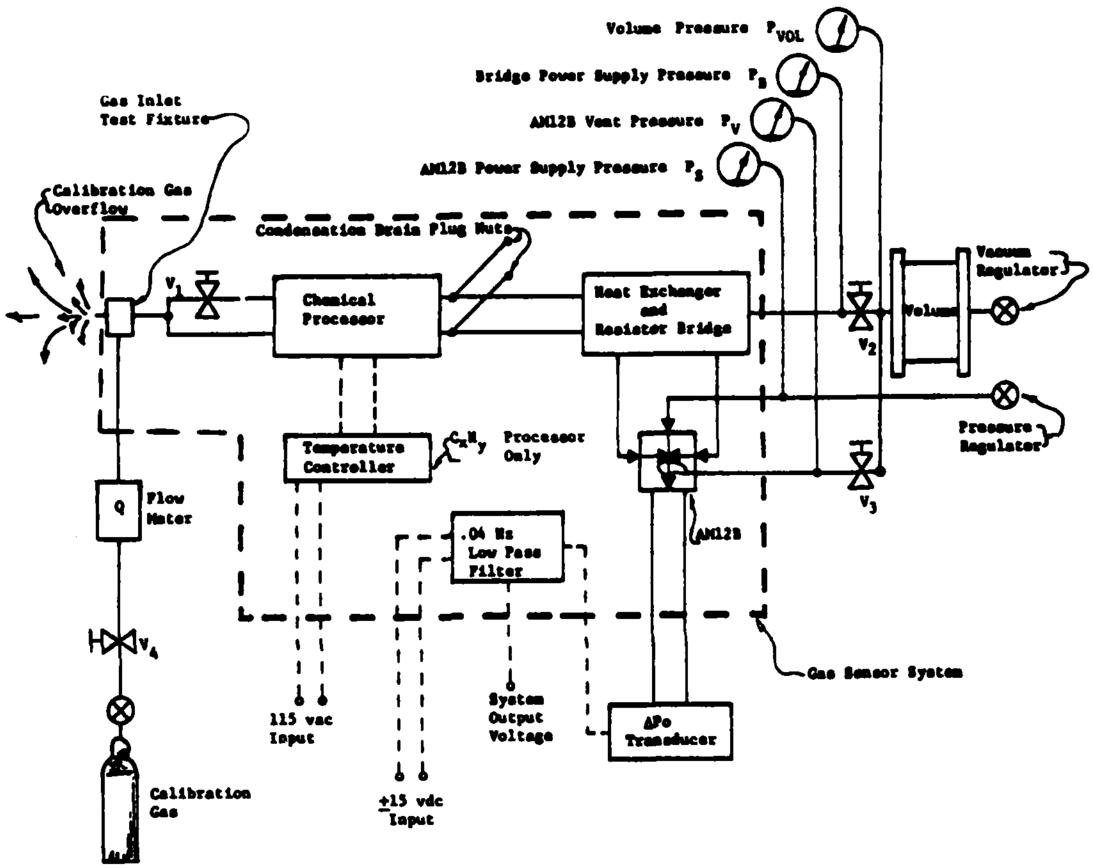

Figure 25. Gas sensor system schematic

from the bridge sensor is amplified by a standard TRITEC five-stage fluidic amplifier (Model AM12B). This amplifier and its active elements are shown in Figure 26. An effective pressure gain of 4500 is produced by the AM12B when coupled to the signal ports of the resistor bridge sensor. This allows the use of an inexpensive electronic pressure transducer to convert the gas pressure signal from the fluidic amplifier into an electrical voltage signal.

With the inlet of the gas sensor system open to the atmosphere, a great deal of noise (from wind, machinery, etc) is induced in the amplified bridge signal. There is also noise caused by the turbulent stages of the fluidic amplifier. This high frequency noise is transmitted to the output of the electronic pressure transducer and reduces the resolution of the sensor system. To remove much of the noise from the sensor system output signal, a 0.04 Hz low-pass filter was constructed from inexpensive electrical components.

The output of the transducer is connected to the electrical filter. The output of the filter can be used to sound an alarm when predetermined gas concentration levels are reached. In addition it can be recorded on an oscillograph so that a time history of gas concentrations is produced.

The hydrogen-sulfide gas sensor system is identical to that for hydrocarbon gas except that the hydrogen sulfide chemical processor with lead acetate flakes (described in Section 4) is used. There is no requirement to produce and control the high chemical-processor temperature needed for catalytic conversion.

With the hydrocarbon-sensor system operating in an environment with a potentially explosive concentration of combustible gases, there is the chance that the catalytic processor itself (operating at a temperature of 400°C) can cause an explosion to occur. Hydrocarbon gas could exist in the atmosphere in an explosive concentration near the catalytic processor. It is possible that if a flame exists in that processor, it could "flash back" through the processor inlet to the atmosphere outside if the proper precautions were not taken.

During this program, several methods for preventing flame fronts from propagating (flashing back) through the inlet flow tubes were investigated. The most universal method used is to reduce the temperature of the flow stream below the point where combustion can occur. This is performed by using coiled metal tubing and metal screening to collect and dissipate excess heat energy.

As was mentioned in Section 4, the temperature of the inlet to the catalytic processor remains near room temperature without the use of special temperature reducing devices. It appears by its low temperature that the inlet tubing to the catalytic-type processor is also serving a heat-dissipating function. As an added precaution, a commercially available flash arrestor was placed between the inlet to the catalytic processor and the sensor system inlet. To provide further protection against flash-

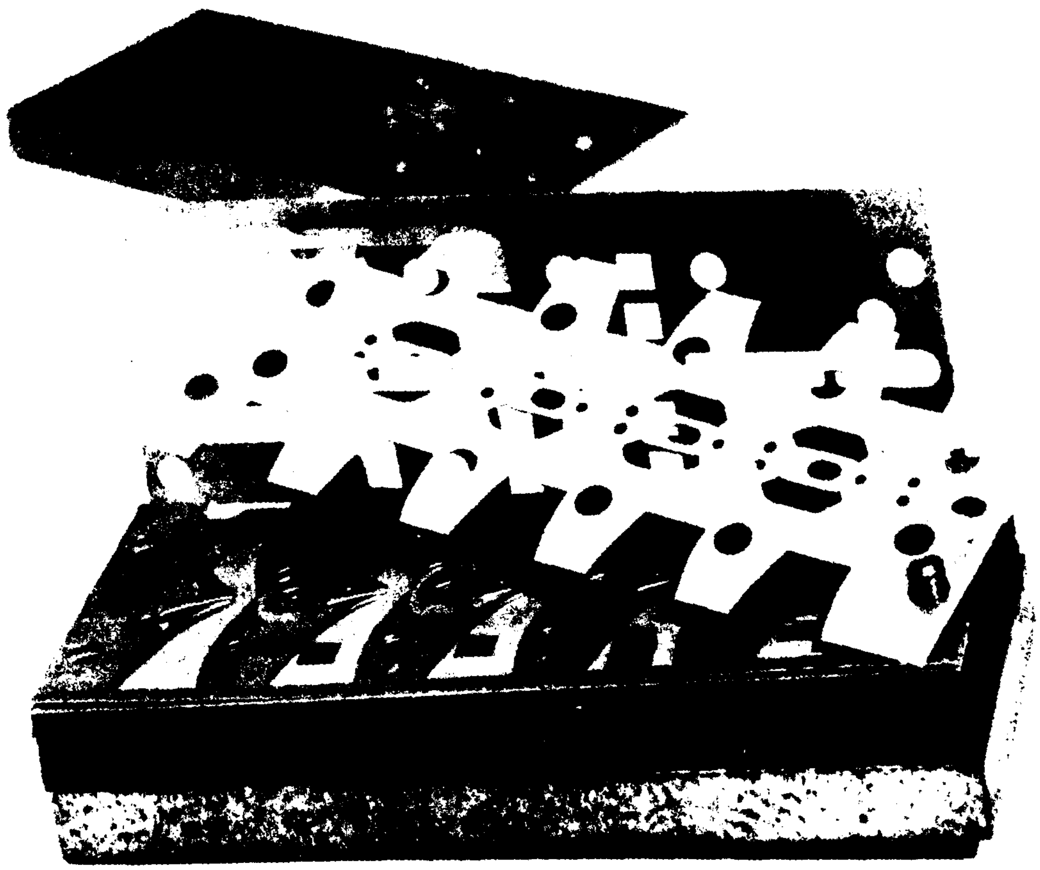

Figure 26 Fluidic amplifier assembly (AM12B)

back, a control in the sensor system could be designed to block the system's inlet and outlet flow paths when a gas concentration near the explosive range is sensed. An alarm could also be sounded to alert all nearby personnel of the danger.

5.2 System Test and Evaluation

Following the assembly of the sensor systems described in section 5.1, tests were conducted to determine their output signal sensitivities to both hydrogen sulfide and methane. These tests utilized commercially available calibrated gas mixtures to provide flow through the chemical processor to the sensor. To avoid introducing these gas mixtures to the sensor system at a pressure other than ambient, and thereby causing a sensor signal null shift or sensitivity change (see Table II), a special test fixture for the gas inlet was designed. It is shown schematically in Figure 25. It consists of a "tee" connected to the calibrated gas supply with one outlet providing flow to the sensor system. The other outlet, consisting of a 6 in. long, 1 in. diameter tube, is open to ambient. Slightly more calibrated gas mixture flows to the "tee" than is drawn off by the sensor system. This provides a constant overflow of the mixture to ambient, insuring that no gas other than the desired mixture is drawn into the sensor. By using the relatively large tube to conduct the overflow to ambient, there is no significant pressure drop between the sensor system inlet and ambient caused by that overflow. Any ambient air diffusing into the inlet will not cause a significant change in gas mixture ratios.

An attempt was made to measure system sensitivity to hydrogen-sulfide gas mixtures. There was no discernable change in output signal level when the mixture concentration was changed from 1 to 50 ppm. This is not unexpected since the testing of the bridge sensor has revealed that its noise level is about ± 120 ppm of CO_2 in N_2, which is theoretically equivalent to ± 111 ppm of H_2S in air. This was more fully discussed in section 2.1.

Figure 27 depicts typical sensor noise data. The short-term noise level is equivalent to ± 49.6 ppm of H_2S in air or ± 50 ppm of methane in air. In addition, there is a long term output signal drift that is equivalent to about ± 25 ppm of methane in air per minute. The drift rate was found to correlate with changes in such operating parameters as sensor power supply level and average gas temperature. Regulation of power supply pressure kept total system noise and drift to an equivalent of about ± 100 ppm of methane in air.

To determine the sensitivity of the hydrocarbon-sensor system, known concentrations of methane in air were used. First, a baseline signal was established by running the sensing system on a methane-in-air gas mixture. Then a different concentration of methane in air was substituted for the first mixture. The signal due to the change in methane concentration is the difference between the system baseline signal and its signal with the second methane gas mixture. The sensor system output signal during a typical sensitivity test run is shown in Figure 28.

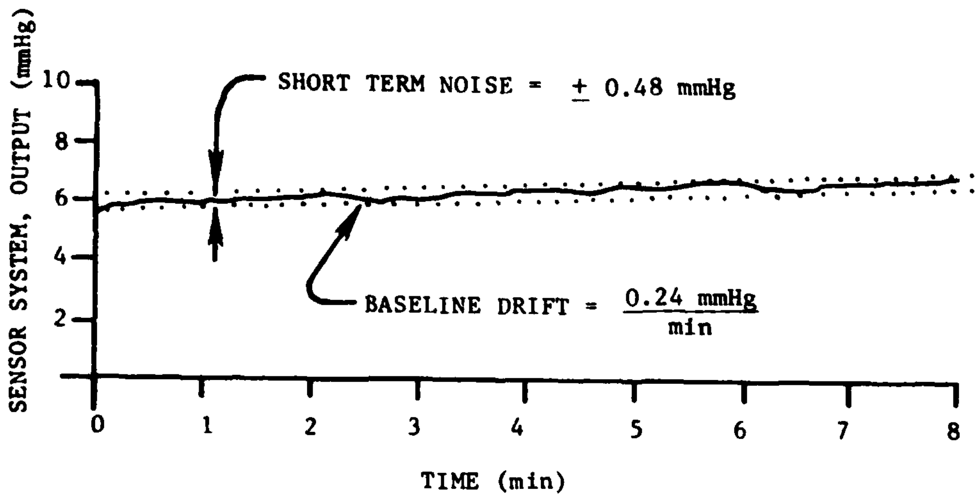

Figure 27. Typical hydrocarbon sensor system noise and baseline drift

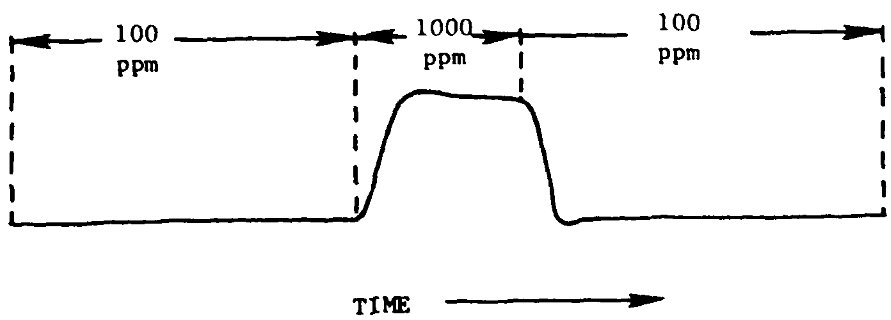

Figure 28. Measurement of typical sensitivity of hydrocarbon sensor system

A series of such tests were conducted and their results combined to obtain a sensor system calibration curve for methane in air. Sensor output level versus the concentration of the methane is presented in Figure 29. This figure shows that the sensor system has a sensitivity of 44 mmHg per percent CH_4 in air.

Tests were performed to evaluate how much drift or signal degradation occurs when a relatively high concentration (more than 1%) of methane is introduced to the sensor system over an extended period of time. These tests showed that, within a half minute, the system signal achieves a steady-state level change corresponding to the sensitivities shown in Figure 29. This level is maintained for about 1-1/2 minutes. The signal then slowly decays toward an indicated zero reading over the next 8-10 minutes. The signal remains steady at this level until some further change in gas concentration occurs. Figure 30 shows a time history of the sensor system signal where the concentration level was changed from 100 to 10,300 ppm methane in air at time $t = 0$ and back to 100 ppm at time $t = 11$ minutes.

Further testing showed that this time dependence of the signal is present at all concentration level changes tested. These ranged from 0.1% to 2.48%.

6. CONCLUSIONS

Although the resistor bridge sensor has more than adequate sensitivity for use in the hydrocarbon sensing system, it has several problems which keep it from sensing H_2S in the 0 to 50 ppm range. The magnitude of its short term signal fluctuations is slightly greater than the signal expected for 50 ppm H_2S in air. In addition, there is sufficient long term baseline drift to cause masking of gas concentration signals in this range. Several possible causes of these problems include

- power supply pressure fluctuations,
- sample gas composition changes,
- gas temperature changes,
- turbulence in the fluidic amplifier, and
- local turbulence in resistor bridge flow paths.

The hydrocarbon sensor system is capable of resolving methane-in-air concentrations from 0.01% (100 ppm) to at least 2.5% with acceptable linearity and repeatability. However, because the sensor signal is a transient one, the sensor system is not yet ready for use as a real time sensor. There are two possible causes for transient behavior:

- transients in the chemical processor reaction and
- temperature transients (either differential or absolute) due to heat release during methane oxidation.

The feasibility of the basic approach has been demonstrated during this effort and a number of problems have been identified. Until

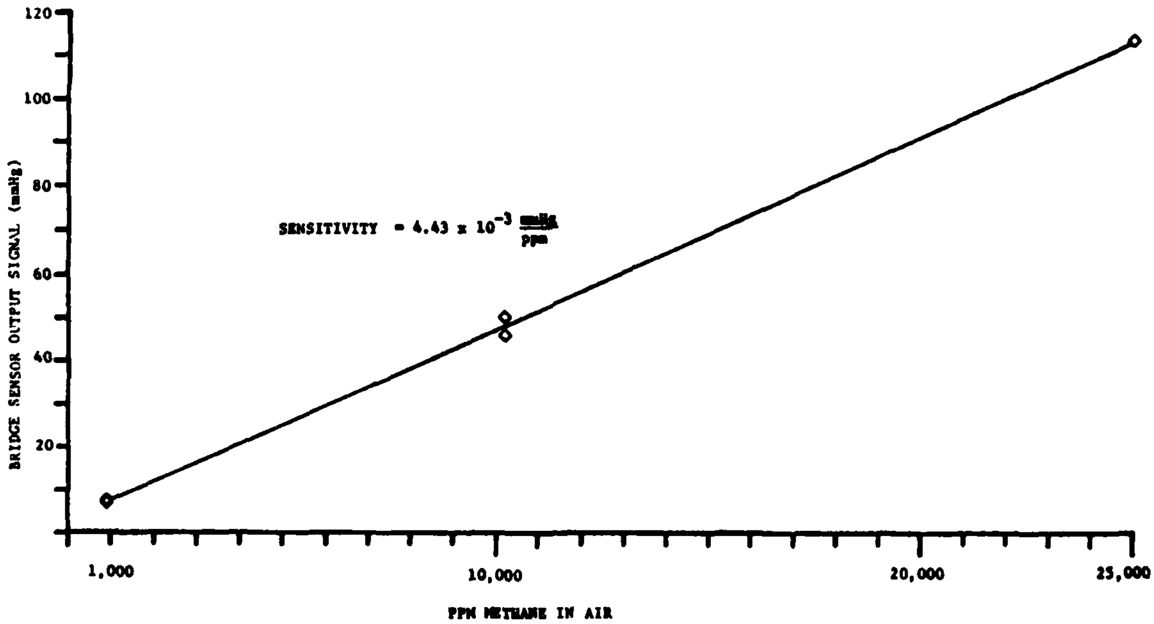

Figure 29. Output signal of hydrocarbon sensor system versus methane concentration in air

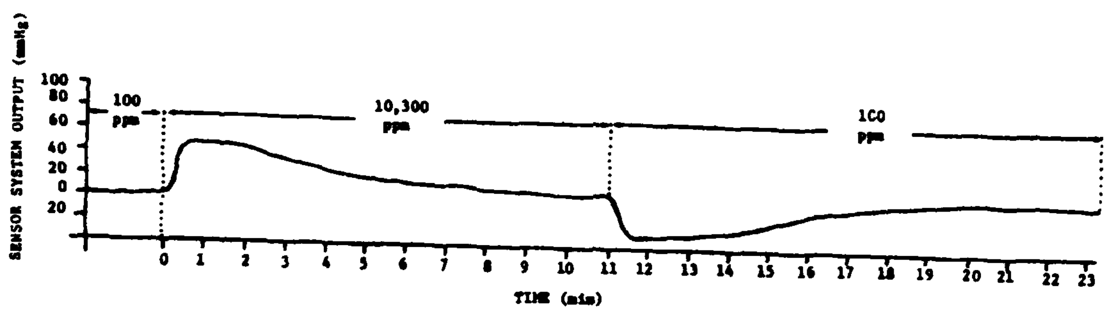

Figure 30. Time history of hydrocarbon sensor system signal

these problems are overcome, the sensor system is not capable of meeting performance goals. The following section outlines a step-by-step approach to address the problems and define the real limitations of this gas sensing system.

7. RECOMMENDATIONS

Two classes of problems are associated with the sensor-system performance. First is sensitivity versus noise level in the sensor-amplifier circuit. The second is the transient nature of the sensor system signal in response to a methane-in-air gas mixture flowing through it.

To reduce the noise in the sensor system signal (and thereby enhance its relative signal sensitivity), there are a number of areas where sensor design can be improved. The sensor system should be fabricated such that the two flow paths are identical to each other, both upstream and downstream of the signal ports (i.e., the total resistance, as well as both the linear and nonlinear components of that resistance are identical). The system then would not be subject to large null shifts caused by power supply pressure fluctuations, absolute temperature changes, or sample gas composition changes.

This ideal can be met with standard fabrication practices if variable resistors that allow independent adjustment of both the linear and nonlinear resistance components are included in the circuit. An alternative approach is to use a second bridge which passes only the sample or the reference gas in both legs to monitor and reduce the inaccuracies caused by the mismatched resistors.

The problems associated with the transient character of the sensor system's response to a methane-in-air gas mixture should be addressed by reevaluation of the design and operating temperature of the chemical processor. In addition, if a temperature differential between the two gas streams is found to be a contributing factor, a redesign of the heat exchanger would be required.

A program which could accomplish these design improvements may consist of the following phases.

- Design and incorporate into the sensor system variable resistors that allow independent adjustment of both the linear and nonlinear resistance components
- Modify bridge sensor to reduce noise and power supply sensitivity
- Optimize matching of fluidic amplifier with bridge sensor

- Improve efficiency of heat exchanger
- Reevaluate and, if required, redesign chemical processors
- Test revised gas sensing systems

LITERATURE CITED

1 Joyce, James W., and Woods, Robert L., "Fluidic Sensors for Life Support Systems," Harry Diamond Laboratories, HDL-TM-75-17, October 1975.

2 Wilke, C.R., "A Viscosity Equation for Gas Mixture," J. Chem. Phys., Vol. 18, No. 4, pp. 517-519, 1950.

3 Gaylord, Wilmer, and Carter, Vondell, "Fluerics 27. Flueric Temperature Sensing Oscillator Design," Harry Diamond Laboratories, HDL-TR-1428, April 1969.

4 Villarroel, Fernando, and Joyce, James. W., "Flueric Carbon Dioxide Concentration Sensor," ASME Paper No. 70-WA/Flcs-10, November 1970.

5 Ostdiek, A.J., "Fluidic Sensors for the Detection of Hydrogen Sulfide Gas and Natural Gas," NEOS, Inc., Report #121, May 1977.

SELECTED BIBLIOGRAPHY

Villarroel, Fernando, and Ragsdale, Charles W., "Army CO_2/O_2 Concentration Monitor (Model 1)," Harry Diamond Laboratories, HDL-TM-7131, December 1971.

Funke, Maurice F., "Flueric System for Sensing Radio-Frequency-Induced Currents," Harry Diamond Laboratories, HDL-TM-69-2, March 1969.

Sheffer, Peter C., and Boyd, J. Michael, "Selective Analysis for Carbon Monoxide, Hydrocarbons, and Nitric Oxide in a Stream of Internal Combustion Engine Exhaust Gases: A Literature Survey," Harry Diamond Laboratories, HDL-TM-76-15, August 1976.

DISTRIBUTION

ADMINISTRATOR
DEFENSE DOCUMENTATION CENTER
ATTN DDC-TCA (3 COPIES)
CAMERON STATION, BUILDING 5
ALEXANDRIA, VA 22314

US GEOLOGICAL SURVEY
EGS-MAIL STOP 620
ATTN JOHN GREGORY (20 COPIES)
RESTON, VA 22092

HARRY DIAMOND LABORATORIES
ATTN TECHNICAL REPORTS BRANCH, 81300
ATTN CHAIRMAN, EDITORIAL COMMITTEE
ATTN PUBLIC AFFAIRS OFFICER
ATTN CHIEF, 13400 (10 COPIES)
ATTN RECORD COPY, 81200
ATTN HDL LIBRARY, (3 COPIES)81100

DATE

ILME

-8